POZNAN UNIVERSITY OF TECHNOLOGY

FACULTY OF COMPUTING AND TELECOMMUNICATIONS
Institute of Radiocommunications

Master's thesis

INFLUENCE OF RF FRONT-END NONLINEARITY ON M-MIMO OFDM SYSTEM

Marcin Wachowiak, 135670

Supervisor
dr hab. inż. Paweł Kryszkiewicz

POZNAŃ 2022

Streszczenie

Systemy Massive MIMO stanowią kluczową technologię sieci 5G, która umożliwia sprostanie rosnącym wymaganiom na przepływność sieci bezprzewodowych. W praktycznych systemach często stosowane są wzmacniacze o ograniczonej liniowości, co w połączeniu z techniką wielotonową OFDM oraz techniką wieloantenową M-MIMO, może powodować, że nadawany sygnał będzie podlegał silnemu zniekształceniu przez nieliniowości stopni wyjściowych. W pracy zbadano wpływ zniekształcenia nieliniowego na efektywną charakterystykę promieniowania i jakość sygnału odbieranego w systemie. Jako model nieliniowości został zastosowany ogranicznik amplitudy, natomiast kierowanie wiązki odbywało się za pomocą prekodowania maksymalizującego moc w punkcie odbioru (ang. Maximum Ratio Transmission - MRT). Otrzymane wyniki pozwalają zaobserwować podobną efektywną charakterystykę kierunkową zarówno dla sygnału pożądanego jak i zniekształceń w przypadkach kanału bezpośredniej widzialności jak i kanału dwuścieżkowego. Następnie zaproponowana została metoda odbioru iteracyjnego redukująca szum przycinania dla systemu wieloantenowego (ang. Multi-antenna Clipping Noise Cancellation- MCNC). Symulacje komputerowe potwierdzają, że odbiornik ten umożliwia efektywną redukcję wpływu nieliniowości na jakość sygnału odbieranego w systemie M-MIMO dla wszystkich sprawdzonych rodzajów kanałów. Zaproponowano również metodę uproszczoną, nie wymagającą informacji o zastosowanym prekodowaniu. W przypadku kanałów bezpośredniej widoczności i kanału dwuścieżkowego uzyskiwana jakość odbioru jest nieznacznie gorsza niż w przypadku algorytmu MCNC. Przedstawione wyniki pozwalają na jakościowe określenie zysków przetwarzania wynikających z zastosowania algorytmów w odbiorniku.

Abstract

Massive MIMO systems are considered a key enabler of the 5G networks, which allows for meeting the growing demands for the throughput in wireless networks. In practical implementations of wireless systems amplifiers with low linearity are often used, which combined with the OFDM technique and M-MIMO technology may result in significant distortion of the transmitted signals by the nonlinear front-end. In this work, the impact of the front-end nonlinearity on the radiation pattern and the received signal quality is studied. The nonlinearity was modelled as a soft-limiter, while the precoding was performed with Maximum Ratio Transmission (MRT). Obtained results show that the radiation pattern is similar both for the desired and distortion signal components in cases of line-of-sight and two-path propagation. In this work, a Multi-antenna Clipping Noise Cancellation (MCNC) algorithm is proposed, which eliminates the performance penalty. By taking into consideration the precoding, the MCNC receiver enables an effective reduction of the influence of non-linearity on the quality of the received signal in a multi-antenna scenario. Next, the performance of the Clipping Noise Cancellation (CNC) algorithm in a multi-antenna scenario was assessed. Based on the computer simulations, it was observed that for the direct visibility channels, the CNC receiver works correctly with only a slight performance degradation. Presented simulation results allow for the qualitative evaluation of the processing gains of both algorithms in regard to several parameters.

Contents

1 Introduction **1**

1.1 Importance of Wireless Communications 1

1.2 Key enabling technologies of the latest and future mobile networks 2

1.3 Multiple antenna techniques in wireless communications 3

1.4 Nonlinearity in wireless systems 4

1.5 Aims and objectives 5

2 Massive MIMO OFDM system **7**

2.1 System model 7

2.2 Simulation framework 12

2.3 Preliminary results 13

3 Influence of front-end nonlinearities on M-MIMO OFDM system **15**

3.1 Literature review 15

3.2 Single user precoding 16

3.3 Multiple user precoding 21

4 Iterative receiver for M-MIMO OFDM system under front-end nonlinearities **23**

4.1 Literature review 23

4.2 Simple reception 24

4.3 Multi-antenna Clipping Noise Cancellation algorithm (MCNC) 24

4.4 Clipping Noise Cancellation algorithm (CNC) 26

4.5 Computational complexity 28

4.6 Simulation results 30

5 Summary **39**

5.1 Conclusions 39

5.2 Future works 40

Acronyms **41**

Bibliography **43**

Chapter 1

Introduction

1.1 Importance of Wireless Communications

Wireless connectivity and the presence of cellular networks have profoundly influenced the global lifestyle and the way humans interact. Having access to a broadband network full of services and entertainment deemed smartphones to become a basic good. The rising demand for throughput and connectivity can be seen in the development trends of the previous and future generations of wireless networks. Starting from the second generation of cellular networks (2G) the main effort was focused on providing greater throughput and efficiency to facilitate the use of Internet services on mobile devices. The demand for higher data rates and capacity in wireless networks seems insatiable. The current deployment of the fifth generation of cellular networks (5G) is destined to meet the growing requirements, but only temporarily as research works have already begun on the next generation, which is the 6G.

According to Ericsson Mobility Report, [13] 5G mobile subscriptions are expected to surpass 1 billion in 2022 and by the end of 2027, their number should reach 4.4 billion. The report also observed that mobile network traffic has doubled in the last two years, a trend which is expected to hold in the coming years. Figure 1.1 presents the global trends in regard to mobile data traffic.

The Internet report by Cisco [4] and the mobility report by Ericsson [13], clearly highlight the

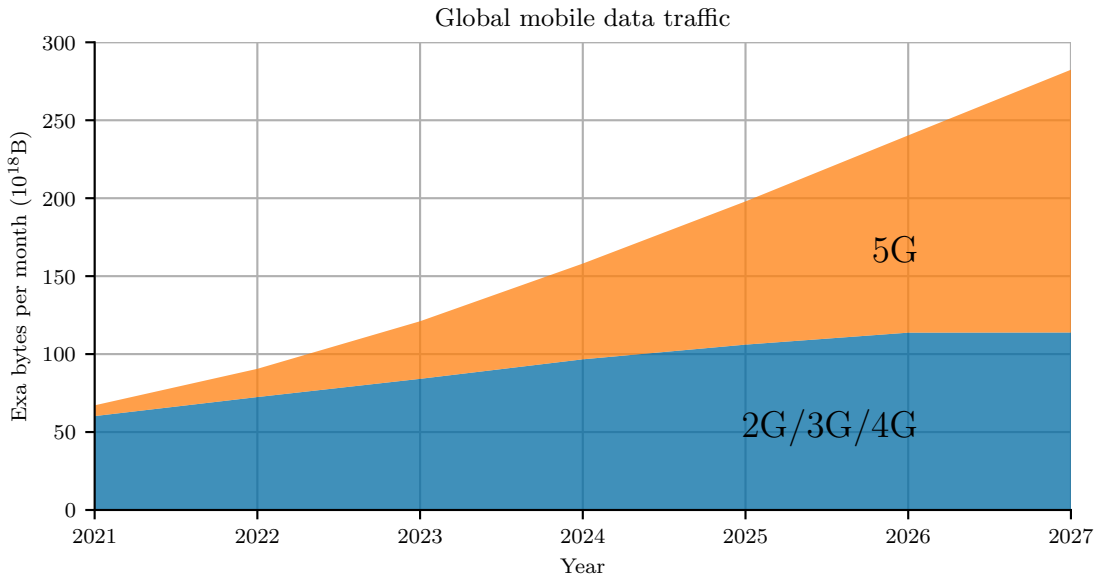

Figure 1.1: Global mobile data traffic prediction according to Ericsson Mobility Report 2022 [13].

need for continuous improvement in the domain of wireless technologies to meet the rising demands of modern, digital societies. It is worth presenting the technical milestones of 5G to give a sense of the scale of the challenge.
Key features of the currently deployed 5G according to ITU-R [37]:

- User data rates of 100 Mbit/s and peak data rate of 20 Gbit/s
- 100x improved network energy efficiency, 10x prolonged battery life and 3x better spectrum efficiency in regard to the previous generation
- Latency of 1ms and supported mobility of up to 500 km/h
- Area traffic capacity of 10 Mbit/s/m^2 (1000x more compared to the previous generation)
- Up to 1 billion connected devices per square kilometer including the Internet of Things (IoT)

1.2 Key enabling technologies of the latest and future mobile networks

To support the objectives set for the 5G in presence of the limited radio resources, a number of novel technologies and approaches had to be introduced [8],[2],[18]:

- Densification of cellular networks with a focus on heterogeneity and coexistence of multi-tier networks. Massive adaptation of small cells.
- Massive MIMO (M-MIMO) utilizing arrays equipped with tens of antennas and advanced signal processing technologies such as 3D-beamforming, space-time precoding or successive interference cancellation. The use of M-MIMO allows exploiting spatial diversity to facilitate Spatial Division Multiple Access (SDMA).
- Utilization of millimeter wave (mmW) frequencies for new communication bands. Previously unexploited frequency ranges above 24 GHz, are to be used in small cells to create high-throughput, short-range links that should efficiently offload the traffic from higher-tier cells.
- Cloud-Based Radio Access Network (CRAN), shifting the base-band processing to the servers at the edge and introducing joint processing mechanisms to reduce the delays and operational costs.
- Network Virtualization, decoupling the network infrastructure from the physical resources, allowing for better utilization of computational and hardware resources resulting in improved network performance. The network functions are also virtualized regardless of the vendor hardware improving scalability and interoperability.
- Green communications based on energy harvesting or renewable resources. Employing energy-aware communication schemes like simultaneous wireless information and power transfer. Aiming to reduce the carbon footprint of the telecommunications industry.

With the start of research works concerning the sixth generation of wireless networks it might be interesting to list the technologies, which are envisioned for it [34], [41], [15]:

- Integration of Machine Learning (ML) and Artificial Intelligence (AI) techniques in the multiple layers of wireless systems, from network management and power allocation to signal processing.

- Utilization of terahertz frequencies and visible light communications for short-range and high-throughput links.
- Use of Large Intelligent Surfaces as reflectors beamforming the reflected signals to provide coverage and better QoS in challenging environments.
- Wireless energy transfer and harvesting for sensors and implants connectivity.
- Integrated terrestrial, airborne and satellite networks for extended coverage and adaptive offloading in hot spots. Providing the access to the network everywhere and at any time.
- Large-scale multi-user Spatial Modulation MIMO (SM-MIMO). Further increase in the number of antennas resulting in Extreme M-MIMO for capacity boost. The possible introduction of the Cell-Free paradigm with M-MIMO.

1.3 Multiple antenna techniques in wireless communications

From the listed key enablers of the 5G, Massive MIMO appears to be one of the most interesting. A high number of transmitting and receiving antennas provides additional degrees of freedom which can be exploited with signal processing to improve the efficiency and performance of wireless transmission systems. Only in the last decade, M-MIMO systems have gained overwhelming interest from academia and industry. The gains stemming from the utilization of antenna arrays in the communications are dependent on the selected transmit (TX) and receive (RX) processing algorithms. MIMO systems offer a wide range of processing methods with their gains and trade-offs [25]:

- Spatial multiplexing techniques – rely on splitting the information sequence into orthogonal streams, which are simultaneously transmitted. The number of streams depends on the properties of the channel and the minimum number of the TX and RX antennas. The main aim of this technique is to provide higher throughput by employing parallelization of data streams.
    - Bell-Labs Layered Space-Time Architecture (BLAST) – the data stream is divided into a number of streams by a multiplexer, each of them fed to a different antenna. Variants proposed later: Vertical (V-BLAST) and Diagonal (D-BLAST) included different spatial mapping of the bits improving the performance [35].
    - Precoding at the transmitter – with the knowledge of the channel state information it is possible to eliminate the interference among the multiplexed signals. One example of such method is Zero-Forcing precoding [23].
    - Successive Interference Cancellation (SIC) – by applying QR factorization of the channel matrix the receiver is able to use its multiple antennas to detect multiple symbols simultaneously and then decode the symbols sequentially while removing the inter-symbol interference caused by previously detected symbols.
- Spatial diversity techniques – aim to improve the error performance of the link. The robustness is achieved by sending precoded copies of the same signal over multiple antennas, which are subject to different propagation. At the receiver, the signals combine resulting improved signal-to-noise ratio, which translates into enhanced performance of the system.
    - Space-Time Trellis Codes (STTC) – scheme uses a generalization of trellis-coded modulation to multiple antennas. The decoding can be performed with the Viterbi algorithm.

  - Orthogonal Space-Time Block Codes (OSTBC) – are based on the mathematical theory of orthogonal designs. The vectors of the precoding matrix are orthogonal to each other, which allows for simpler linear and optimal decoding at the receiver.

- Beamforming techniques – can be interpreted as linear filtering in the spatial domain. Knowing the geometry of the array and the radio environment by varying phase shifts or amplitude multipliers between antenna elements it is possible to maximize the array gain in the desired direction.

  - Digital beamforming – each antenna is connected to an individual digital baseband processing front-end. This solution guarantees the greatest flexibility with the highest cost and complexity of hardware in regard to other solutions.
  - Hybrid beamforming – the number of digital transceivers is lower than the number of antennas, the precoding is done partially in the digital domain and partially with the use of phase shifters.
  - Analog beamforming – a single digital processing front-end is used to generate a signal that is distributed to antenna elements equipped with phase shifters, which allow to steer the beam.

With Massive MIMO, the performance of the above-mentioned techniques can be leveraged even further due to the greater number of antennas. Figure 1.2 presents an illustrative case of beamforming with M-MIMO array, which is shaping the radiation pattern in the direction where the receiving device is located. Figure 1.3 present an illustration of the transmit diversity in M-MIMO system. The channels between the transmit antennas vary, which can be exploited to improve the robustness of the wireless link.

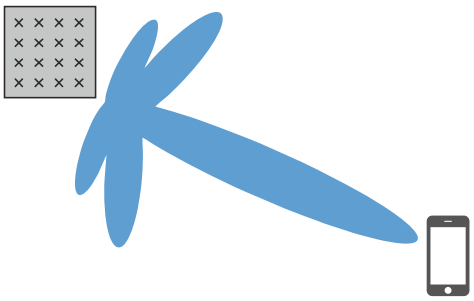

FIGURE 1.2: Beamforming in M-MIMO.

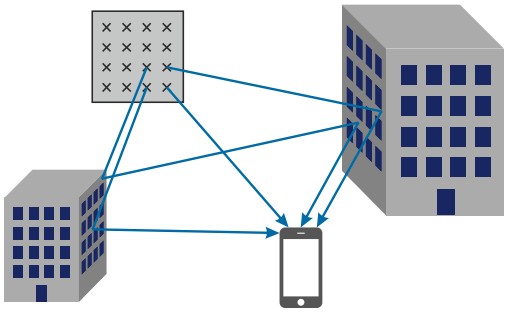

FIGURE 1.3: Transmit diversity in M-MIMO.

1.4 Nonlinearity in wireless systems

Nonlinearity in wireless systems originates from the nonlinear components and devices, which are incorporated into the design of the transmitter or receiver. The main radio front-end blocks that introduce the most nonlinear distortion are amplifiers and mixers. The Power Amplifiers (PA) are responsible for the power amplification of the signal to make it suitable for transmission over the wireless channel. Ideally, the PA gain would be constant across all input powers. However, in practical PA the output power is limited by the DC input power, therefore the gain decreases while the input power is increased. Depending on the input power range the operation of the amplifier can be considered linear for low input powers and nonlinear when operating close to the saturation region. It is usually desirable to operate the PA in the saturation region as it allows to obtain

the maximum power efficiency [14] at the cost of introducing nonlinear distortion for signals with varying amplitude.

Due to nonlinearity, the signal at the output of a PA contains unwanted signal components referred to as nonlinear distortion. The nonlinear distortion is manifested as harmonics at multiples of signal frequencies when the signal consists of discrete tones or as spectral regrowth when the input signal has a finite bandwidth. The additional signal components are called intermodulation products. The presence of in-band distortion components degrades the performance of the system, while the out-of-band components may interfere with other wireless systems and similarly affect their performance. The influence of the nonlinearity on the signal can be characterized by the input signal Peak-to-Average Power Ratio (PAPR) [6]. The greater the PAPR the more significant the nonlinear distortion of the signal. High values of PAPR cause the input signal to drive the amplifier more into the saturation region resulting in a higher contribution of the nonlinear effects.

1.5 Aims and objectives

The aim of this work is to study the influence of nonlinear distortion on a Massive MIMO system employing Orthogonal Frequency-Division Multiplexing (OFDM). The radiation characteristic of a M-MIMO array with front-end nonlinearity is analyzed both for wanted and distortion signals and its impact on the receiver performance is evaluated. Finally, two iterative distortion recovery algorithms are proposed and tested in the multi-antenna scenario and their gains are discussed.

Objectives:

- Perform a detailed study on the influence of the front-end nonlinearity on Massive MIMO systems backed up by theoretical analysis and simulation results.
- Investigate the radiation characteristic of the desired and distortion signal components in a uniform linear array (ULA) and evaluate the Signal Distortion Ratio (SDR) for selected channel models.
- Evaluate the Bit Error Rate (BER) performance and the spectral characteristic of the received signals in the M-MIMO system in the presence of nonlinearity.
- Propose an iterative reception algorithm for reduction of nonlinear distortion and test its performance in a multi-antenna scenario. Propose a simplified algorithm to allow distortion cancellation with reduced computational complexity and reduced amount of control information.

Structure of the work

The rest of this work is structured as follows, second chapter presents the theoretical formulation of the system model used throughout the work. The simulation framework is mentioned and some preliminary results are shown. Next, the third chapter is focused on analyzing the effective radiation characteristics of the M-MIMO arrays with nonlinear front-ends. Among others, the beam patterns of desired and distortion signal components are discussed. In the fourth chapter, the proposed iterative distortion recovery receivers are presented. The chapter is concluded with a presentation of simulation results regarding the performance of the reception algorithms. Final remarks and conclusions are given in the fifth chapter.

Chapter 2

Massive MIMO OFDM system

2.1 System model

A transmission system depicted in Fig. 2.1 is considered. There are N_{U} QAM symbols s_n ($n \in \{1, ..., N_{\mathrm{U}}\}$ transmitted over adjacent subcarriers in a single OFDM symbol period. The modulation symbols are chosen from set χ. The symbols are precoded and transmitted by K parallel transmitting signal chains, each consisting of an OFDM modulator with a maximum number of N subcarriers, a nonlinear amplifier and an antenna element. Signals from different antennas combine at the single antenna receiver. The next subsections describe the signal processing in each of the functional blocks.

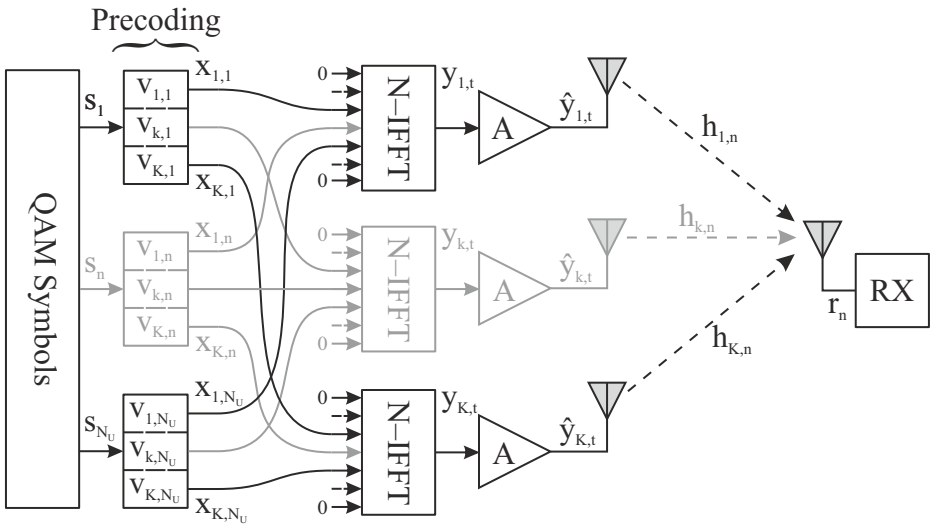

FIGURE 2.1: System model.

Radio channel

In order to utilize the OFDM modulator, it is assumed that the radio channel is constant for the frequency span of a single subcarrier, i.e., channel coherence bandwidth is not smaller than a single subcarrier bandwidth. For n-th subcarrier and k-th antenna, the channel response is a single complex coefficient expressed as $h_{k,n}$.

Considered radio channels types :

- Line-of-Sight (LOS): modeled as attenuation of the free space and phase rotation resulting from the distance between the transmitter and receiver.
- Two-path: apart from the direct path it includes an additional one corresponding to the reflection from the ground with a reflection coefficient equal to -1. The point of reflection is calculated taking into consideration the location of the RX and TX elements.
- Rayleigh: modeled as independent, identically distributed complex Gaussian variables for each subcarrier, antenna and azimuth.

Precoding

Precoding is applied by multiplying the data symbol at n-th subcarrier s_n by precoding coeffcient $v_{k,n}$ for n-th subcarrier and k-th antenna obtaining the precoded symbol $x_{k,n}$:

$$x_{k,n} = s_n v_{k,n}. \tag{2.1}$$

It is assumed that the precoder is normalized to obtain a unitary summarized transmit power gain, irrespective of the number of utilized antennas for each subcarrier independently, i.e.,

$$\sum_{k=1}^{K} |s_n v_{k,n}|^2 = |s_n|^2 \sum_{k=1}^{K} |v_{k,n}|^2 = |s_n|^2 . \tag{2.2}$$

For a special case of maximum ratio transmission (MRT), which maximizes the received power, the precoding coefficients are calculated as [23]:

$$v_{k,n} = \frac{h_{k,n}^*}{\sqrt{\sum_{\tilde{k}=1}^{K} \left| h_{\tilde{k},n} \right|^2}}, \tag{2.3}$$

where $*$ denotes complex conjugate.

OFDM Modulation

Precoded symbols are then subject to OFDM modulation, which is performed by Inverse Fast Fourier Transform (IFFT) of size N. Only N_{u} subcarriers of indices $\mathcal{N}$ are modulated by data symbols $x_{k,n}$. The other $N - N_{\mathrm{U}}$ subcarriers are modulated with zeros. Typically, for a symmetric OFDM spectrum and an unused DC subcarrier the subcarrier indices set equals $\mathcal{N} = \{-N_{\mathrm{u}}/2, ..., -1, 1, ..., N_{\mathrm{u}}/2\}$. The output of the IFFT t-th sample of OFDM signal for k-th antenna is calculated as:

$$y_{k,t} = \frac{1}{\sqrt{N}} \sum_{n \in \mathcal{N}} x_{k,n} e^{j 2\pi \frac{n}{N} t}, \tag{2.4}$$

where $t \in \{-N_{\mathrm{CP}}, ..., N-1\}$, and N_{CP} is the number of samples of the cyclic prefix (CP).

Nonlinear amplifier

The modulated signal is processed by a nonlinear amplifier model identical for each transmitting signal chain:

$$\hat{y}_{k,t} = \mathcal{A}(y_{k,t}), \tag{2.5}$$

which in the case of the soft limiter can be described as:

$$\hat{y}_{k,t} = \begin{cases} y_{k,t} & \text{for } |y_{k,t}|^2 \leq P_{\max} \\ \sqrt{P_{\max}} e^{j \arg(y_{k,t})} & \text{for } |y_{k,t}|^2 > P_{\max} \end{cases}, \tag{2.6}$$

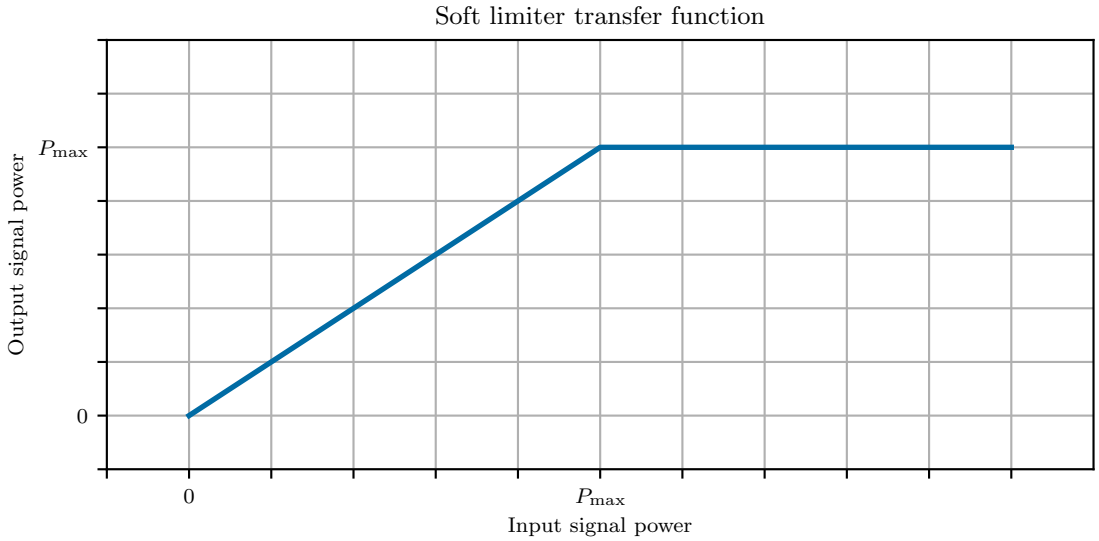

FIGURE 2.2: Soft limiter transfer function.

where $P_{\max}$ is the maximum transmit power of a given Power Amplifier (PA) and $\arg(y_{k,t})$ denotes phase of $y_{k,t}$. If exceeded, the signal is clipped, i.e., has constant amplitude while maintaining the input phase. While there is a number of different PA models, the soft limiter is proved to be the nonlinearity maximizing the signal-to-distortion ratio [31]. While in many contemporary systems digital pre-distortion is employed, the soft limiter can be treated as an optimal characteristic of the combined PA and pre-distorter model. Figure 2.2 presents a soft limiter transfer function shape.

It is a common practice to use Input Back-off (IBO) parameter to determine PA operating point and respectively the $P_{\max}$. It is defined as a ratio of maximum PA power to the average power at the input of the amplifier, expressed in decibels scale:

$$IBO\ [dB] = 10log_{10}\left(\frac{P_{\max}}{\mathbb{E}[|y_{k,t}|^2]}\right), \tag{2.7}$$

where the expectation operator is denoted as $\mathbb{E}$.

Assuming that the average signal power is calculated based on an individual OFDM symbol samples over all antennas and using (2.2) it is obtained:

$$\mathbb{E}[|y_{k,t}|^2] = \frac{\bar{P}_s}{NK}\sum_{n\in\mathcal{N}}\sum_{k=1}^{K}|v_{k,n}|^2 = \frac{\bar{P}_s N_{\mathrm{u}}}{KN}, \tag{2.8}$$

where $\bar{P}_s$ is the average power of a single symbol s_n. If the wireless channel is varying in time the expectation over $|v_{k,n}|^2$ should be also considered. Because of averaging mean power over antennas in (2.8) all K amplifiers work with the same clipping threshold $P_{\max}$.

The signal at the output of the amplifier can be decomposed based on the principle of homogenous linear mean square estimation [28] as:

$$\hat{y}_{k,t} = \alpha_k y_{k,t} + \bar{d}_{k,t}, \tag{2.9}$$

where α_k is the correlation coefficient specific for k-th antenna, $\bar{d}_{k,t}$ is the distortion signal uncorrelated with the desired signal $y_{k,t}$. The coefficient α_k is defined as follows:

$$\alpha_k = \frac{\mathbb{E}\left[\hat{y}_{k,t}y^*_{k,t}\right]}{\mathbb{E}\left[y_{k,t}y^*_{k,t}\right]}. \tag{2.10}$$

The value α_k can be derived analytically assuming a complex-Gaussian distribution of $y_{k,t}$ [33]. While an exact signal envelope distribution for QAM-modulated OFDM is of discrete nature [40], it converges fast with the number of subcarriers to its limit, i.e., a complex-Gaussian distribution. This comes from the utilization of the central limit theorem as $N_{\mathrm{U}} \gg 0$ independently modulated subcarriers are used. In [39] it has been shown that the limit distribution is obtained not only for independent and identically distributed symbols. It is valid as well for the coded system, allowing the modulating symbols to be dependent but uncorrelated. Additionally, power variation among subcarriers, e.g., as a result of water filling, still allows the complex-Gaussian distribution to be used. These derivations allow the complex-Gaussian assumption to be valid for the M-MIMO OFDM system. First, while various precoders $v_{k,n}$ can be used, e.g., MRT of ZF [23], these typically depend on the wireless channel properties, not the modulating symbols resulting in $\forall_{n\in\mathcal{N}}\mathbb{E}[s_n v_{k,n}] = \mathbb{E}[s_n]\mathbb{E}[v_{k,n}]$. As such, using a common assumption that QAM symbols are uncorrelated of zero mean, i.e., $\forall_{n\neq m}\mathbb{E}[s_n s_m^*] = \mathbb{E}[s_n]\mathbb{E}[s_m^*]$ and $\mathbb{E}[s_n] = 0$, it can be shown that

$$\forall_{n\neq m}\mathbb{E}[x_{k,n}x_{k,m}^*] = \mathbb{E}[s_n]\mathbb{E}[s_m]^*\mathbb{E}[v_{k,n}v_{k,m}^*] = 0. \tag{2.11}$$

Therefore, the symbols $x_{k,n}$ are uncorrelated as required by [39]. The second issue is the power variation among subcarriers. It can happen as a result of some sort of water filling, resulting in $\exists m \neq n\mathbb{E}[|s_n|^2] \neq \mathbb{E}[|s_m|^2]$. However, it is possible that power amplification by coefficient $v_{k,n}$ can vary among subcarriers, e.g., in the case of MRT precoder as a result of frequency selective fading. Still, [39] shows the complex-Gaussian assumption can be used in these cases.

As such α_k can be calculated as in [33] considering that power can be unequally distributed among antennas, e.g., as a result of some antenna array elements being pointed in different directions than the served user, resulting in the increased power of other matrix elements for an MRT precoder described by (2.3). In case of a common maximal transmit power $P_{\max}$ for all utilized front-ends, mean TX power per antenna can be different resulting in varying per-antenna IBO, i.e.,

$$IBO_k\ [dB] = 10log_{10}\left(\frac{P_{\max}}{\frac{\bar{P}_s}{N}\sum_{n\in\mathcal{N}}|v_{k,n}|^2}\right), \tag{2.12}$$

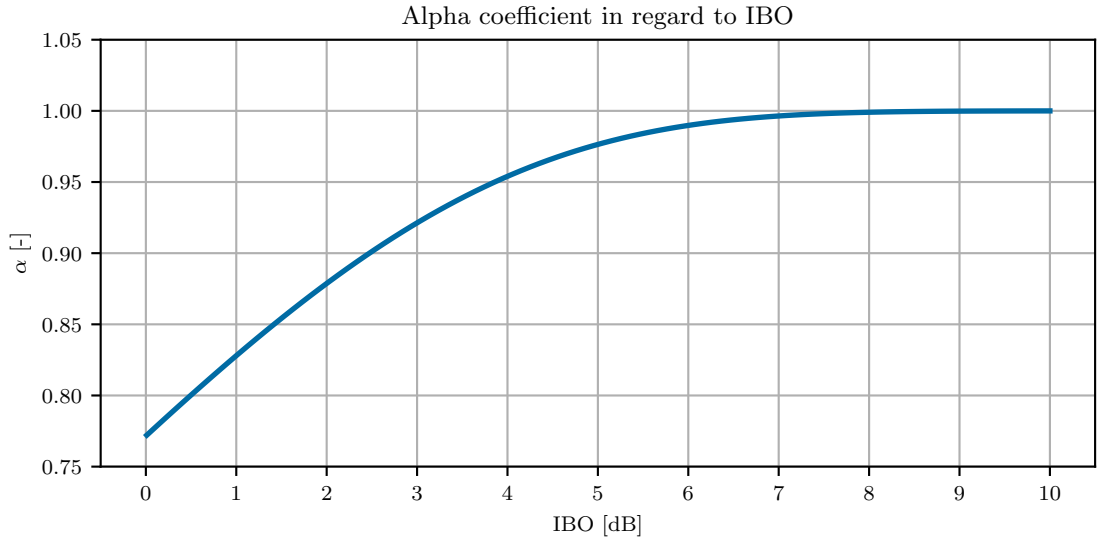

FIGURE 2.3: Value of the alpha coefficient in regard to IBO according to analytical formula (2.13).

The coefficient α_k can be calculated as [33]:

$$\alpha_k = 1 - e^{-\gamma_k^2} + \frac{\sqrt{\pi\gamma_k}}{2}\,\mathrm{erfc}\,(\gamma_k), \tag{2.13}$$

where $\gamma_k = 10^{\frac{IBO_k}{20}}$ and erfc$(\cdot)$ denotes the error function. Observe that in many architectures and for many channel types the coefficient α_k will be invariant with respect to the antenna index.

Figure 2.3 presents the values of the α according to the analytical formula in (2.13) for IBO in the range 0–10 dB. For high values of the IBO the alpha coefficient is approximately equal to unity. The low IBO corresponds to the value of α lower than one, meaning that the power of the undistorted signal component is accordingly decreased.

Signal reception

The signal transmitted in time domain $\hat{y}_{k,t}$ from k-th antenna is convolved with its respective wideband channel. After passing through the channel the K signals are summed at the receiving antenna. After removal of CP, the Fast Fourier Transform (FFT) is applied which allows expressing the signal received at n-th subcarrier as:

$$r_n = \sum_{k=1}^{K} \mathcal{F}_{[n,t=0,\ldots,N-1]}\{\hat{y}_{k,t}\} h_{k,n} + w_n, \tag{2.14}$$

where w_n is the white noise sample at n-th subcarrier in the receiver and $\mathcal{F}_{[n,t=0,\ldots,N-1]}\{\cdot\}$ denotes Discrete Fourier Transform (DFT) over time instants $t = 0, ..., N-1$ at n-th subcarrier.

Based on (2.9) and (2.4) the received signal can be expanded to:

$$r_n = \sum_{k=1}^{K} \alpha_k h_{k,n} x_{k,n} + \sum_{k=1}^{K} h_{k,n} d_{k,n} + w_n, \tag{2.15}$$

where

$$d_{k,n} = \mathcal{F}_{[n,t=0,\ldots,N-1]}\{\bar{d}_{k,t}\}. \tag{2.16}$$

Observe that in general $d_{k,n}$ for a single subcarrier depends on the transmitted symbols s_n and precoding coefficients $v_{k,n}$ for all the utilized subcarriers $n \in \mathcal{N}$. This can be easily shown by treating OFDM signal as a set of subcarriers undergoing intermodulation on a polynomial-modeled PA [10].

Taking into account the precoding coefficients definition in (2.1) it is obtained that

$$r_n = \sum_{k=1}^{K} \alpha_k h_{k,n} v_{k,n} s_n + \sum_{k=1}^{K} h_{k,n} d_{k,n} + w_n. \tag{2.17}$$

The Signal-to-Noise Ratio (SNR) is defined considering only the data-carrying subcarriers with the wanted signal attenuated by coefficients α_k giving

$$SNR = \frac{\bar{P}_s \frac{1}{N_u} \sum_{n\in\mathcal{N}} \left| \sum_{k=1}^{K} \alpha_k h_{k,n} v_{k,n} \right|^2}{\mathbb{E}\left[|w_n|^2 \right]}. \tag{2.18}$$

Based on the SNR definition the Eb/N0 can be calculated as:

$$\frac{Eb}{N0} = \frac{SNR}{\log_2 M}, \tag{2.19}$$

where M is the size of the constellation.

Similarly, the Signal-to-Distortion Ratio (SDR) is defined considering only the data-carrying subcarriers:

$$SDR = \frac{\bar{P}_s \sum_{n\in\mathcal{N}} \left|\sum_{k=1}^{K} \alpha_k h_{k,n} v_{k,n}\right|^2}{\sum_{n\in\mathcal{N}} \left|\sum_{k=1}^{K} h_{k,n} d_{k,n}\right|^2}. \tag{2.20}$$

2.2 Simulation framework

To evaluate the performance M-MIMO system in the presence of the front-end nonlinearity a simulation framework was implemented. The framework was implemented using Python programming language based on the object-oriented programming paradigm. Division of transmission system elements and functional blocks into classes allowed for simplification of the simulation scripts and provided much-needed scalability. Where possible signal processing operations were performed with the use of matrices, Numpy library and Numba a high-performance Python compiler to speed up the computations.

The key parameters of the considered M-MIMO system are shared within all analyses and simulation scenarios. The transmitting end was a uniform linear array with an inter-element spacing of half wavelength. Each antenna was modeled as an omnidirectional radiator with a gain of 0 dBi. The arrangement of antenna elements can be seen in Fig. 2.4 where the azimuth angle is denoted as θ. The transmitter end was positioned at 15 m above ground level. Tab. 2.1 presents the details concerning the transmission system. Each front-end amplifier was modeled as a soft limiter with an identical cutoff power. A single receiver was placed 300 m from the TX at an azimuth of 45° and 1.5m above the ground level. The perfect Channel State Information (CSI) known both at the transmitter and receiver is assumed. The antenna array transmitters employ MRT precoding.

Table 2.1: Transmission system parameters

Parameter	*Symbol*	*Value*	*Unit*
Subcarrier spacing	Δf	15	[kHz]
Carrier frequency	f_c	3.5	[GHz]
Total number of subcarriers	N	4096	[−]
Number of data subcarriers	N_{U}	2048	[−]
QAM constellation size	M	64	[−]

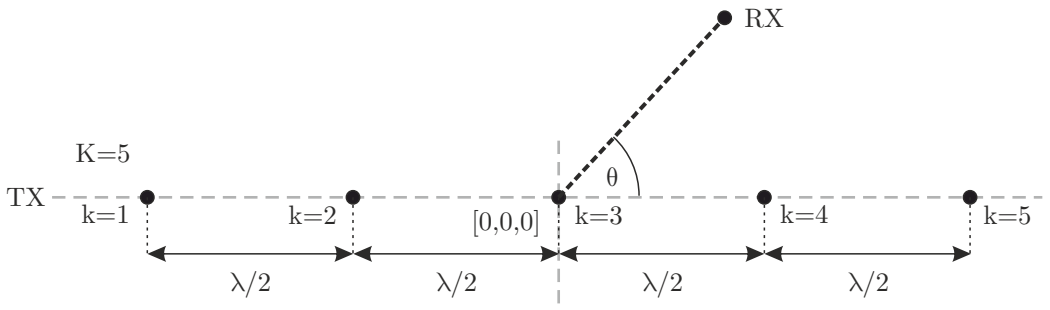

Figure 2.4: Antenna array arrangement with azimuth angle denoted as θ.

2.3 Preliminary results

To gain insight into the properties of the transmitted signal Power Spectral Sensity (PSD) an analysis for Single-Input Single-Output (SISO) system was first performed. For an uncoded single antenna system 100 OFDM frames were transmitted and collected to calculate the PSD at the output of the amplifier model. The model of nonlinear distortion was the soft limiter and the measurement was performed for a few values of the IBO. Figure 2.5 shows the relative PSD of combined signal at the output of the transmitter and Fig. 2.6 presents the relative PSD of the desired and distortion signal components in regard to the IBO.

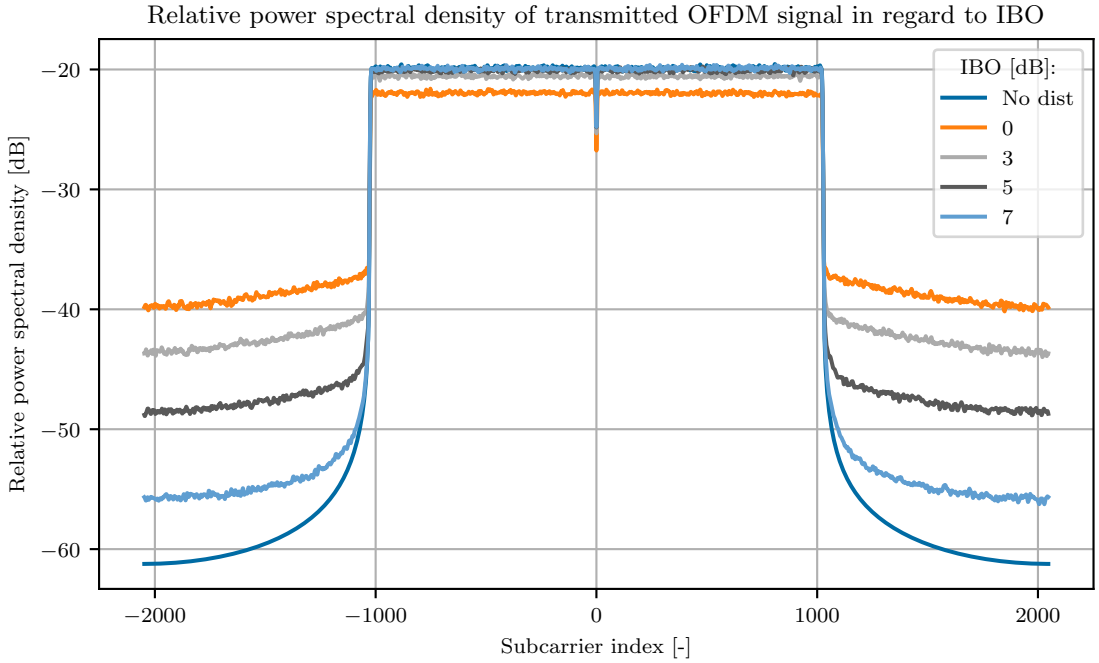

FIGURE 2.5: Relative power spectral density of the transmitted OFDM signal for selected IBO values.

The split of the transmitted signal into the respective desired and distortion components was achieved with Bussgang decomposition from (2.9). The figures show that low values of IBO, which correspond to severe clipping of the signal, cause a significant spectral regrowth both in-band and out of the signal band region. For severe clipping, the power of the desired signal is scaled accordingly to the square of the α parameter, which value is equal to 1.0 when there is no nonlinear distortion and decreases with increasing IBO accordingly to (2.13). As the signal power needs to be conserved the power from the in-band region is transferred into the adjacent bands in the form of out-of-band interference. Decreasing IBO corresponds to raising the distortion component level, reducing the signal-to-distortion ratio. Another interesting observation is that the SDR is not constant between the subcarriers, due to the shape of the distortion signal PSD, which is similar to a flattened bell curve.

Next, Fig. 2.7 shows values of α_k with respect to IBO_k for IBO = 0 dB, $K = 64$ TX antennas and MRT precoding at an azimuth angle of 45°. Recall that IBO_k is IBO calculated individually for each TX antenna (2.12) considering the utilized precoding vectors while IBO is an overall system and simulation parameter that does not take the precoding into account. It is visible that for all considered channels the α_k values vary slightly among front-ends. Most importantly, it is visible that in all the cases the estimated α_k value follows the analytical result of (2.13) as discussed in Sec. 2.1. The value of α_k depends only on IBO of each individual front-end.

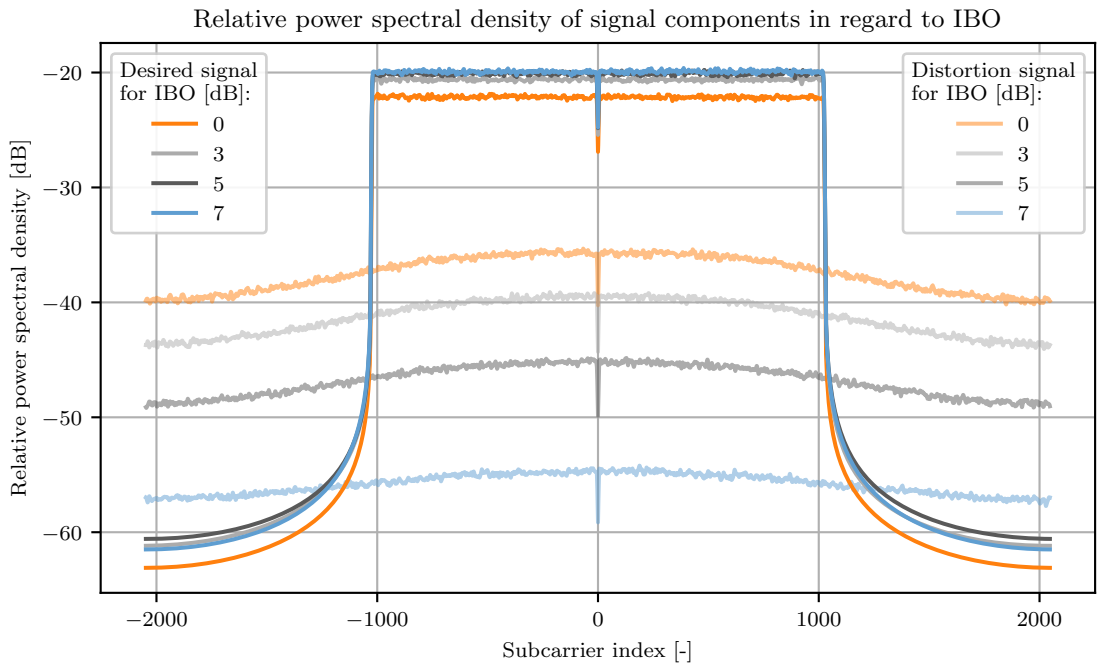

FIGURE 2.6: Relative power spectral density of selected signal components in SISO OFDM system for various IBO values.

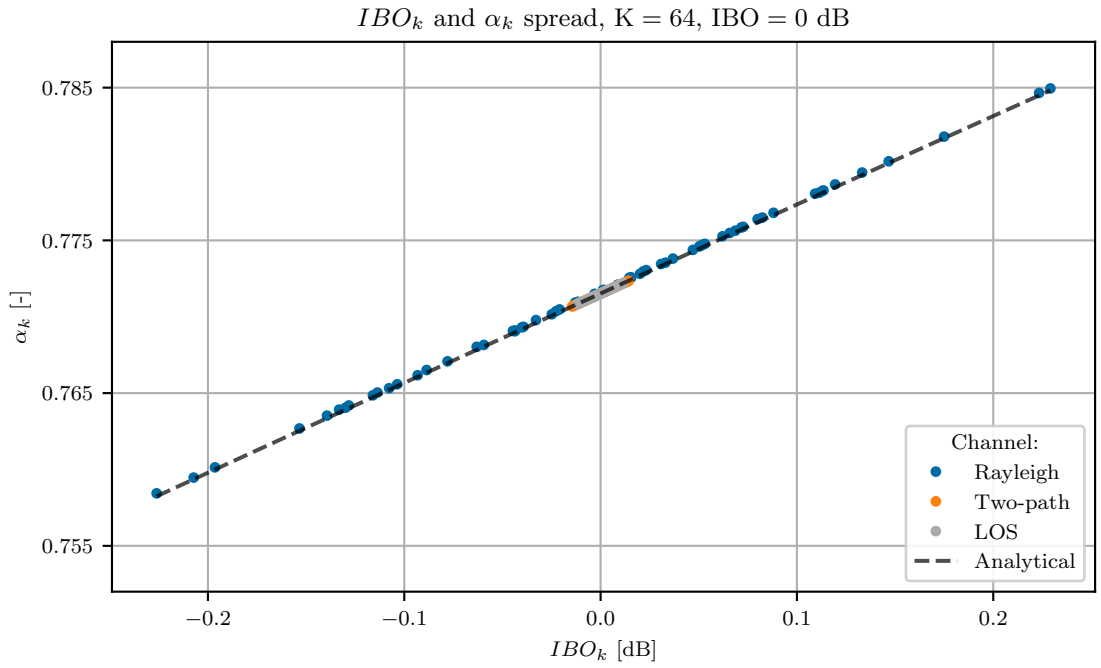

FIGURE 2.7: IBO_k and α_k values of individual antenna front-ends for $K = 64$, IBO = 0 dB, MRT precoding at azimuth angle of 45° and selected channels.

Chapter 3

Influence of front-end nonlinearities on M-MIMO OFDM system

3.1 Literature review

With the advent of Massive MIMO communications, the problem of nonlinear distortion reappears in a new context. The presence of nonlinearity in a multi-antenna scenario introduces an additional degree of complexity, which has to be carefully considered. Most of the terrestrial MIMO systems employ OFDM modulation due to high bandwidth efficiency and low complexity receiver structure. However, the OFDM modulation is characterized by a high Peak-to-Average Power Ratio (PAPR) [14], which combined with nonlinear amplification results in significant signal distortion. Initial analyses [7] assumed that in multi-antenna systems the distortion can be modeled as additive white noise. This would lead to omnidirectional radiation of the distortion signal, even in the presence of precoding, which would be a very favorable scenario. Later, on the contrary, the analysis in [21] has proven that in some scenarios the distortion signals across different antennas are in fact correlated and the former claim is erroneous. Consequently, the distortion adds up constructively in distinct spatial directions. That analysis was performed in a multi-antenna system with two subcarriers and nonlinearity modeled as a third-order polynomial. For single-user precoding it was shown that the distortion is beamformed in the same direction as the desired signal, however, for multi-user scenarios, the distortion was observed to be beamformed also in directions different from the intended receivers. A follow-up work [5] found that some in-band and out-of-band emissions are always beamformed in the same directions as the desired signals. In [27] a detailed study of the radiation pattern of the distortion and the wanted signal was performed. The authors derived a spatial cross-correlation matrix of nonlinear distortion components, which could be used to predict the expected signal to distortion levels for both in-band and out-of-band. In [26] it was shown that with the growing number of users served simultaneously the distortion signal radiation pattern becomes approximately omnidirectional. The out-of-band components of the distortion signal, which are radiated in directions other than the intended user may degrade the reception quality of other users in the vicinity.

In this section, the radiation patterns of the OFDM signal in the M-MIMO system are examined. Contrary to discussed works, the amplifier nonlinearity is modeled as a soft limiter and the propagation is also studied for a two-path channel model, which was not previously considered.

3.2 Single user precoding

In order to analyze the effective radiation pattern of a M-MIMO system under nonlinearity, a series of simulations were run. Based on the derived system model in Sec. 2.1 the received signals were processed to obtain the components corresponding to the desired and distortion signal. The key simulation parameters were the same as presented in Sec. 2.2. The transmission was precoded for an azimuth angle of 45°. The resolution of the measured polar radiation pattern is 0.1°. For each point on the radiation pattern plot, 10 OFDM symbols were collected to calculate the power of the signal, a number that was deemed accurate during the tuning of the simulation scripts. The desired and distortion signal powers are calculated taking into consideration only the data-carrying subcarriers. For the PSD figures 100 OFDM symbols were collected.

First the radiation beam patterns of desired and distortion signal components in a M-MIMO system are analyzed. A practical but previously not so widely considered channel in the context of the nonlinearity in M-MIMO is the two-path channel model. Fig. 3.1 shows the normalized radiation pattern of the desired and the distortion signal components separately. The normalization was performed in regard to the maximum value of the radiation characteristic. The radiation patterns are highly directional as the array is composed of a high number of antennas. Both the desired and distortion signal components exhibit nearly identical shapes of the radiation pattern. Subtracting the values of the two components the SDR value can be read, which is approximately 19.4 dB for IBO = 3 dB. It is nearly fixed for any azimuth angle. It is worth noting that for the considered uniform linear array there exists a symmetry of the radiation pattern, which allows to skip the plotting for the range from 180 to 360°.

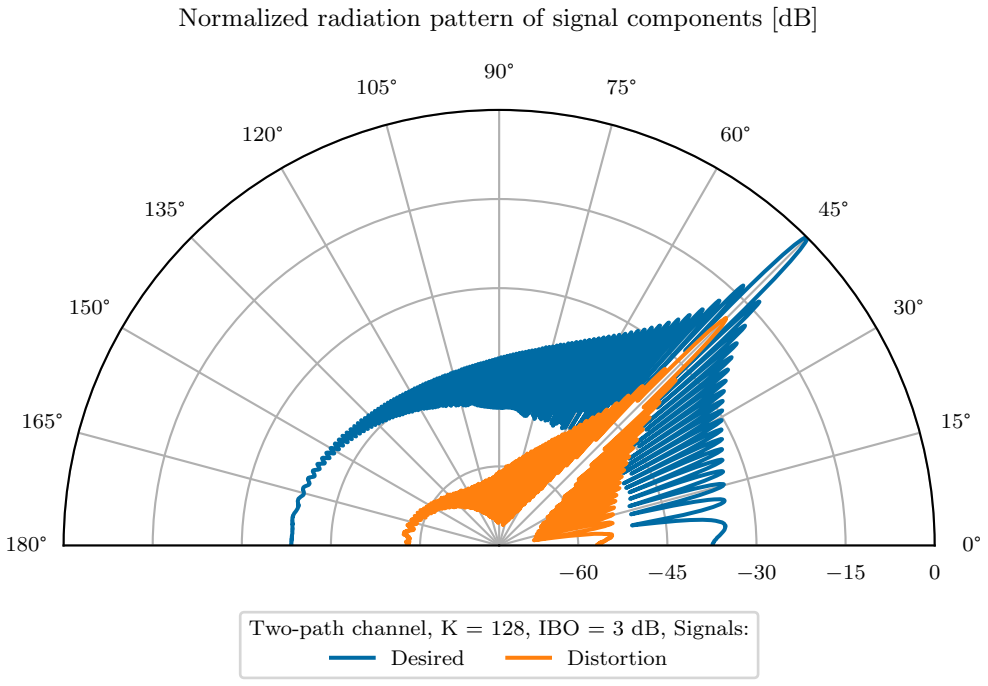

FIGURE 3.1: Normalized radiation pattern of desired and distortion signal components in regard to azimuth angle for two-path channel model, 128 antennas and IBO = 3 dB.

The overall radiation pattern of the array varies in regard to the gain and number of side lobes with the number of antennas. Figure 3.2 presents the measure of the normalized radiation pattern of the distortion signal for a range of 16-128 antennas. It is visible that the more antennas are used the narrower beam can be generated and a higher number of sidelobes is present. Most importantly,

while the radiation patterns of the desired signal are not shown, these have identical shapes as these ones for distortion signals shifted appropriately considering a constant signal-to-distortion ratio.

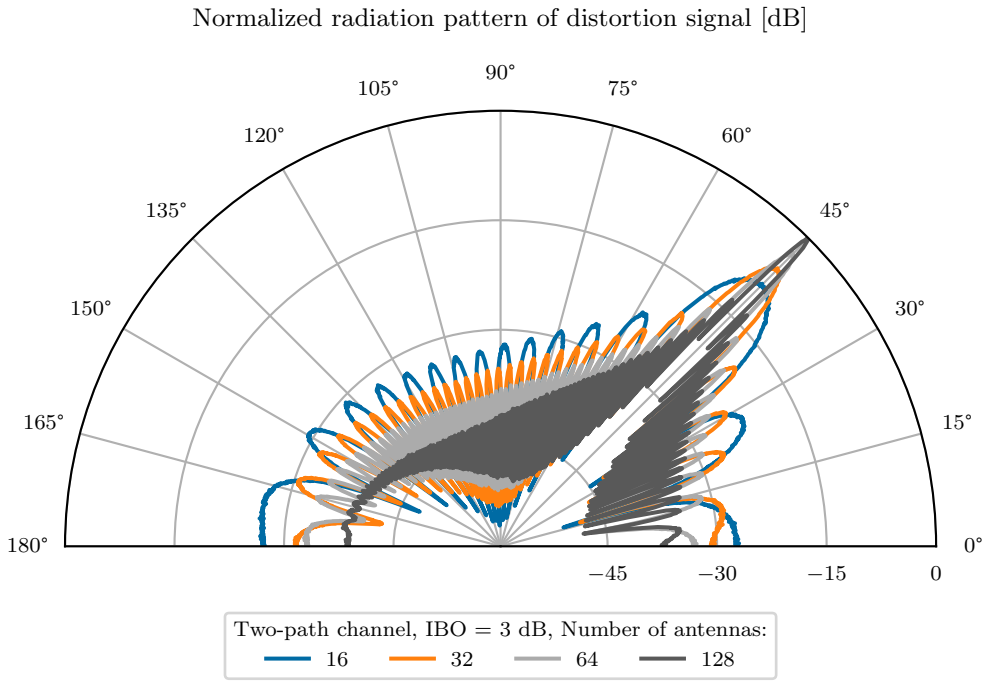

FIGURE 3.2: Normalized radiation pattern of distortion signal in regard to azimuth angle for two-path channel model, IBO = 3 dB and selected numbers of antennas.

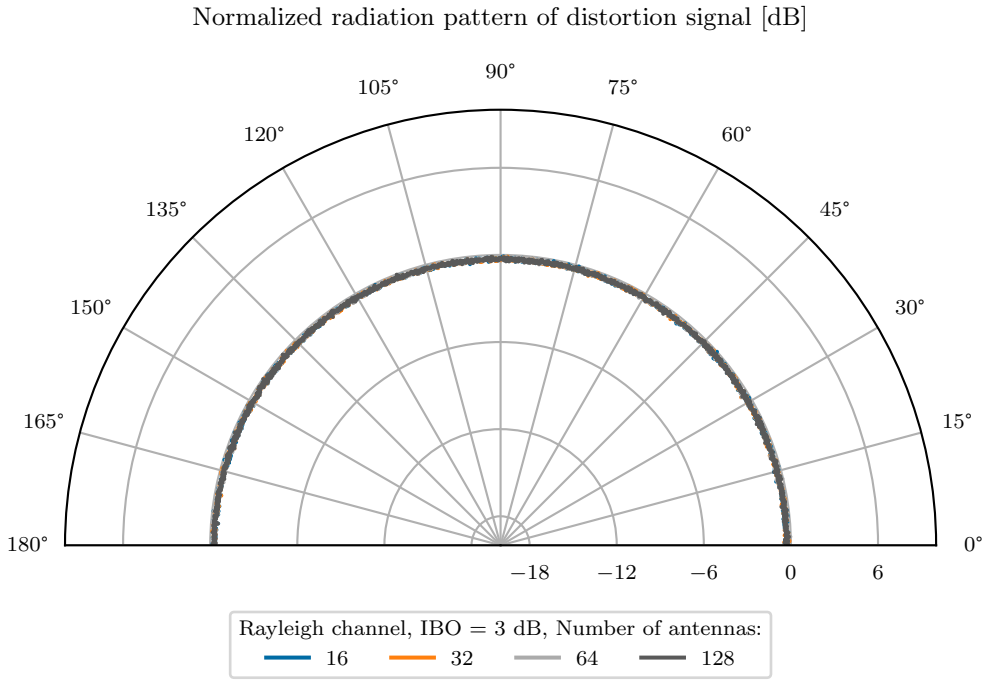

FIGURE 3.3: Normalized radiation pattern of distortion signal in regard to azimuth angle for Rayleigh channel model, IBO = 3 dB, and a selected number of antennas.

In the case of the ideal Rayleigh channel, widely discussed in many publications, e.g. [7], it can indeed be presumed that nonlinear effects may be negligible with a sufficiently large number

of transmit antennas. Figure 3.3 shows the normalized radiation pattern of the distortion signal component. Regardless of the number of antennas and direction of the precoding the distorted signal power is constant for all angles for the Rayleigh channel. The omnidirectional radiation of the distortion signal is beneficial as it is not amplified by the array gain which increases power of the desired signal component at the receiver. However, it must be taken into account that the real radio channels usually deviate from this idealized model [16].

Fig. 3.4 shows the relative power spectral densities of the desired signal and distortion at the intended receiver for the LOS channel, K = 128 antennas and IBO of 3 dB. Both signals retain characteristics similar to that known for the transmitted OFDM signal in a single antenna system. It can be seen that the nonlinear distortion has a wider bandwidth than the desired signal causing both in-band and out-of-band interference.

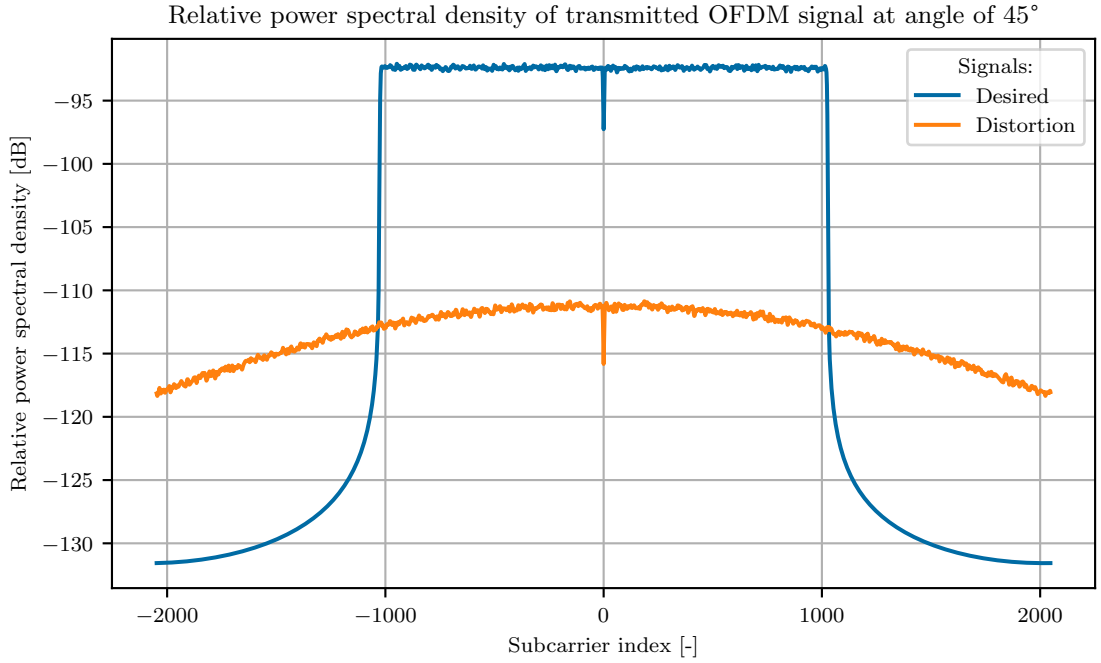

FIGURE 3.4: Relative power spectral density of the desired and distorted signal components at the receiver for the LOS channel model at the precoding angle of 45°, 128 antennas and IBO = 3 dB.

To investigate what is the power spectral density at angles different from the precoding at 45°, a measurement was performed in the same setting for the angle of 54.4°. The selected angle corresponds to the null of the radiation pattern. Fig. 3.5 presents the relative PSD at the selected angle. Apart from the significantly reduced power of the signals, frequency-selective fading can be observed. The curve marking the PSD of the signal without nonlinear distortion and the desired signal component is subject to the same fading, even though it is a LOS channel. This fading is a result of summation in counter phase symbols transmitted from all TX antennas at a given subcarrier. This is a combined effect of precoding and channel propagation. The fading is also present for the distortion signal, however its shape is not exactly the same as for the desired signal component. The nulls of the radiation pattern, where the signal power is highly attenuated, are problematic regions from the numerical simulation perspective. Low levels of the measured signal powers result in low accuracy of the received signal power or SDR making numerical precision errors more visible.

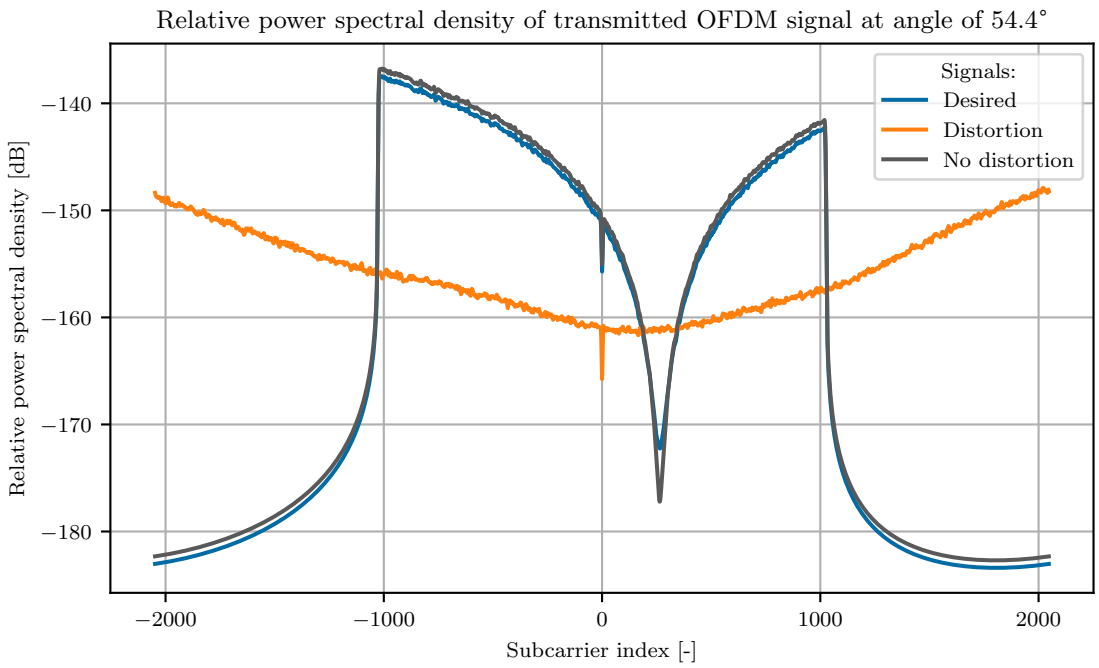

FIGURE 3.5: Relative power spectral density of the desired and distorted signal components at the receiver for the LOS channel model at a different than precoding angle of 54.4°- null of the radiation pattern, 128 antennas and IBO = 3 dB.

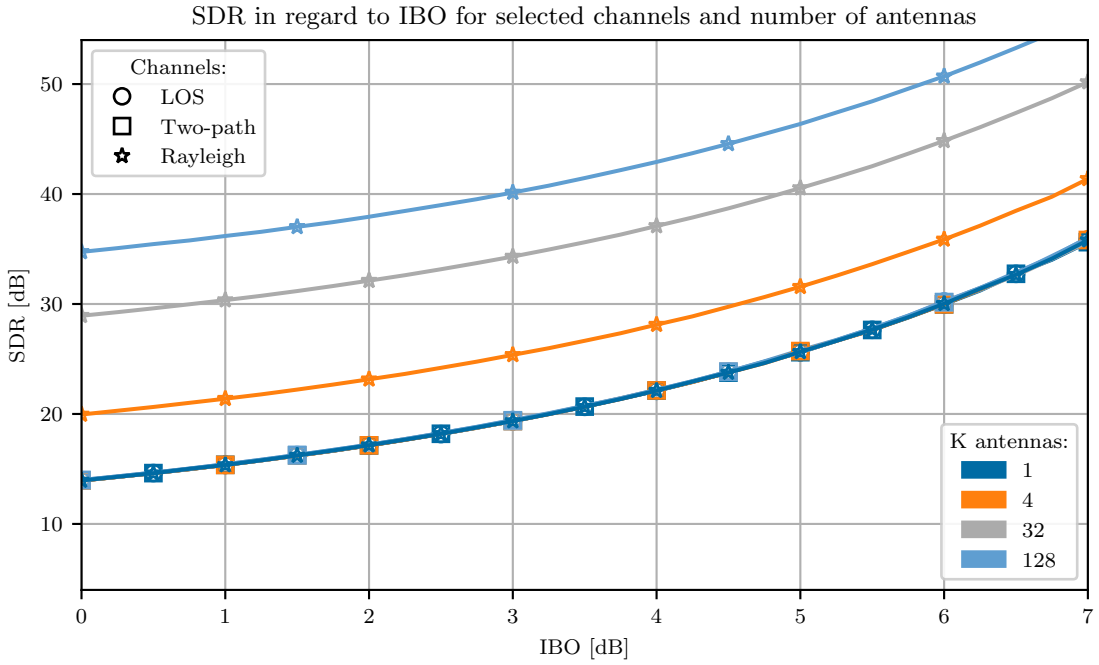

FIGURE 3.6: SDR in regard to IBO for selected channels and number of antennas, for MRT precoding at an azimuth angle of 45°.

Next, the Signal to Distortion Ratio (SDR) analysis was performed for all three considered channels: LOS, two-path and rayleigh and the selected number of antennas. Recall that SDR is calculated taking into consideration only the used subcarriers N_U. The results for all considered channels are shown in Fig. 3.7. The results for the LOS channel agree with the earlier analyzes discussed in the literature review according to which the desired and distorted signal components are directed in the same way, resulting in a constant signal-to-distortion ratio regardless of the

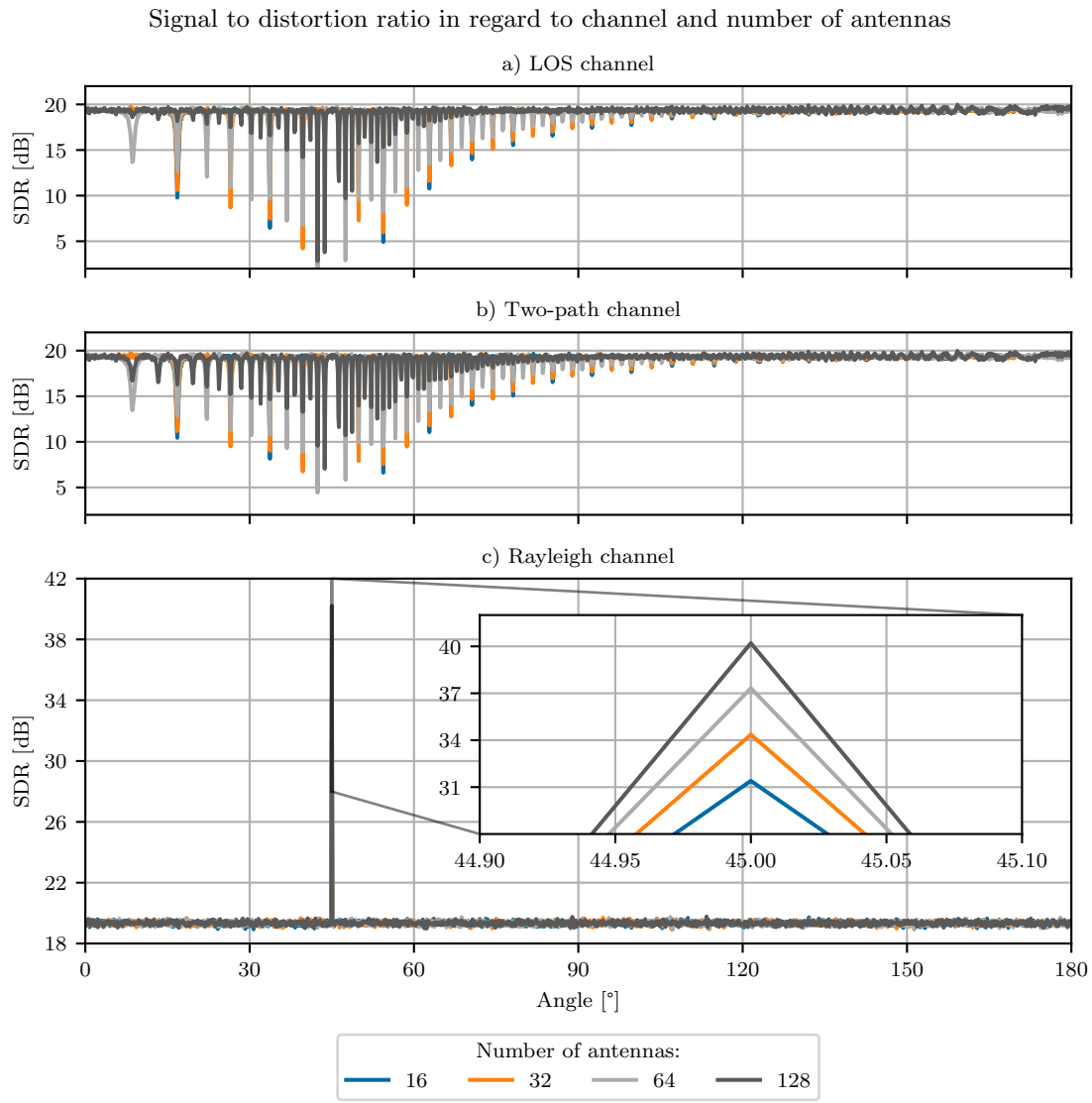

FIGURE 3.7: Signal to distortion ratio in regard to angle and number of antennas for selected propagation channels and IBO = 3 dB.

number of antennas and the azimuth angle used in the precoding. Slight fluctuations in the SDR value dependent on the azimuth or the number of antennas are due to the radiation pattern nulls and limited accuracy of the simulation. For the two-path channel model, the angles and the SDR ratios are very similar to those of the LOS channel. Despite adding an additional path representing the reflection, the signal-to-distortion ratio remains constant for the whole range of angles and number of antennas.

For the Rayleigh channel, a significant increase in the SDR value can be seen for the precoding angle. Due to a lack of correlation between channel coefficients for different antennas and subcarriers the Rayleigh channel exhibits gains in a signal-to-distortion ratio proportional to the logarithm of the number of antennas, $10 \log_{10} K$. At other angles when the precoding vector does not correspond to the actual channel coefficients, no such gain is present.

Figure 3.6 shows the signal-to-distortion ratio plotted against the IBO for selected channels. While the MRT precoding is expected to provide $10 \log_{10}(K)$ dB gain of the wanted signal, at the same time it can increase the power of nonlinear distortion arriving at the receiving antenna [21]. This happens both for LOS and two-path channels as increasing the number of antennas

does not change SDR value. Only for the considered Rayleigh channel, the nonlinear distortion can be reduced by increasing K as expected in [7]. However, keep in mind that the considered Rayleigh channel model is independent and identically distributed both among antennas and subcarriers. A similar effect can be observed if multiple users are served in parallel, improving the SDR performance [27]. This shows that while utilization of the massive number of antennas can combat many phenomenons, e.g., high path-loss or channel fadings, there is still in some scenarios a need for solutions removing the impact of nonlinear PAs. In this work, single-user precoding is considered as it is the case most challenging from a nonlinear distortion perspective.

3.3 Multiple user precoding

The multiple user precoding in a M-MIMO system allows to form of a number of beams in the spatially separated directions where the user terminals are located. It facilitates spatial multiplexing and improves system performance with coverage tailored to the user positions. Although the multi-user precoding is not used in further analysis within this work it might be beneficial to gain some insight into the impact of nonlinearity in this case.

For multiple user precoding the precoded symbols for each user are obtained similarly to (2.1), with the difference that for each user a separate data symbol sequence and precoding vector corresponding to its channel is used:

$$x_{k,n,u} = s_{n,u} v_{k,n,u}, \tag{3.1}$$

where u denotes the user index ($u \in \{1, ..., U\}$) and U is the number of users. The precoded user symbols are then summed:

$$x_{k,n} = \sum_{u=1}^{\mathrm{U}} x_{k,n,u}. \tag{3.2}$$

The resultant combined symbol vector is subject to OFDM modulation. The multi-user precoding introduces a change in the transmitted signal power, which should be accounted for in formulas from the chapter 2.

To investigate the radiation patterns in a multi-user scenario a simulation with 3 users was run. The users were positioned 300 m from the antenna array at angles of 45, 120 and 150° respectively. The angular resolution of the polar radiation characteristic is 0.1°. For each point on the radiation pattern plot, 10 OFDM symbols were averaged to calculate the power of the signals.

Figure 3.8 shows the normalized radiation pattern of the desired and distortion signal components in a multi-user precoding scenario. The desired signal radiation pattern characteristic is similar to that of a single user scenario apart from the fact that there are now 3 peaks at angles where the users are located. The distortion signal radiation pattern can be observed to have multiple peaks in addition to the ones present at the precoding angles. The distortion signal peaks at angles different than precoding may cause harmful interference to the users in the vicinity of the system.

Figure 3.9 presents the signal-to-distortion ratio for the same setting and multi-user precoding compared with the previously analyzed single-user case. It is visible that for multi-user precoding the SDR polar characteristic is far less regular than in a single-user scenario due to the presence of new distortion signal peaks. The SDR at user angles for multi-user precoding is higher by 3 dB compared to single-user cases. This result confirms, that with a greater number of users the nonlinear distortion is far less harmful to the M-MIMO system and at some point can be approximated as omnidirectional radiation [26]. This allows us to emphasize that single-user

precoding, further considered, is indeed the worst-case scenario from the receiver perspective in M-MIMO system.

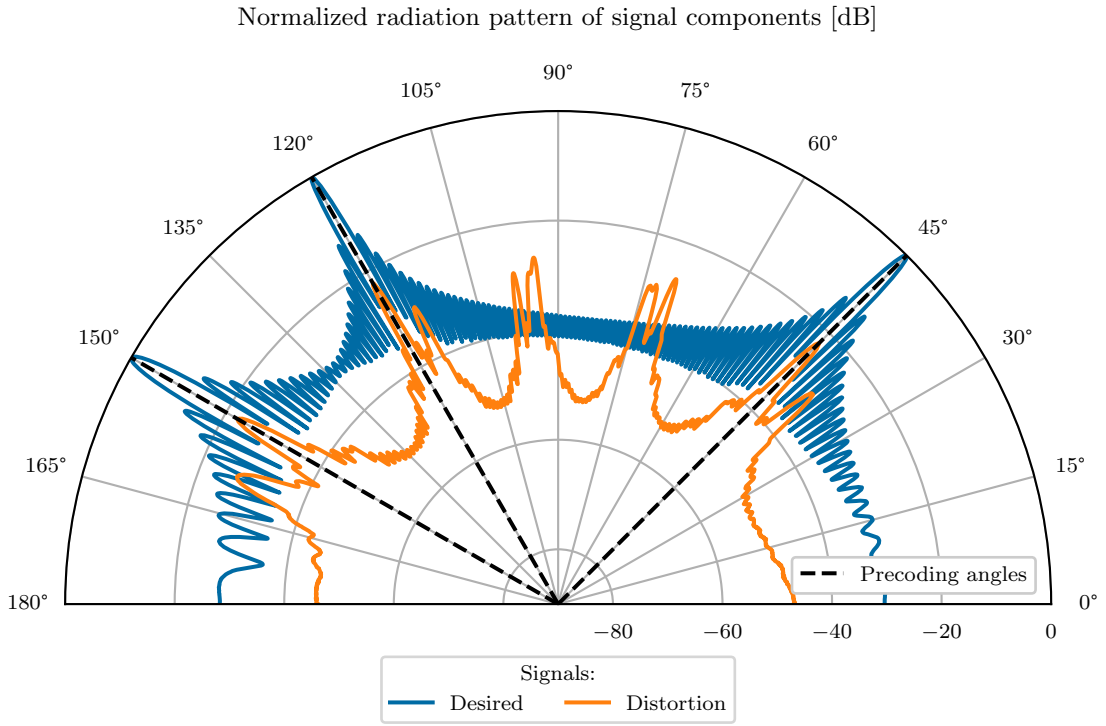

FIGURE 3.8: Normalized radiation pattern of signal components in regard to azimuth angle for multi-user precoding, two-path channel model, IBO = 3 dB and 128 antennas.

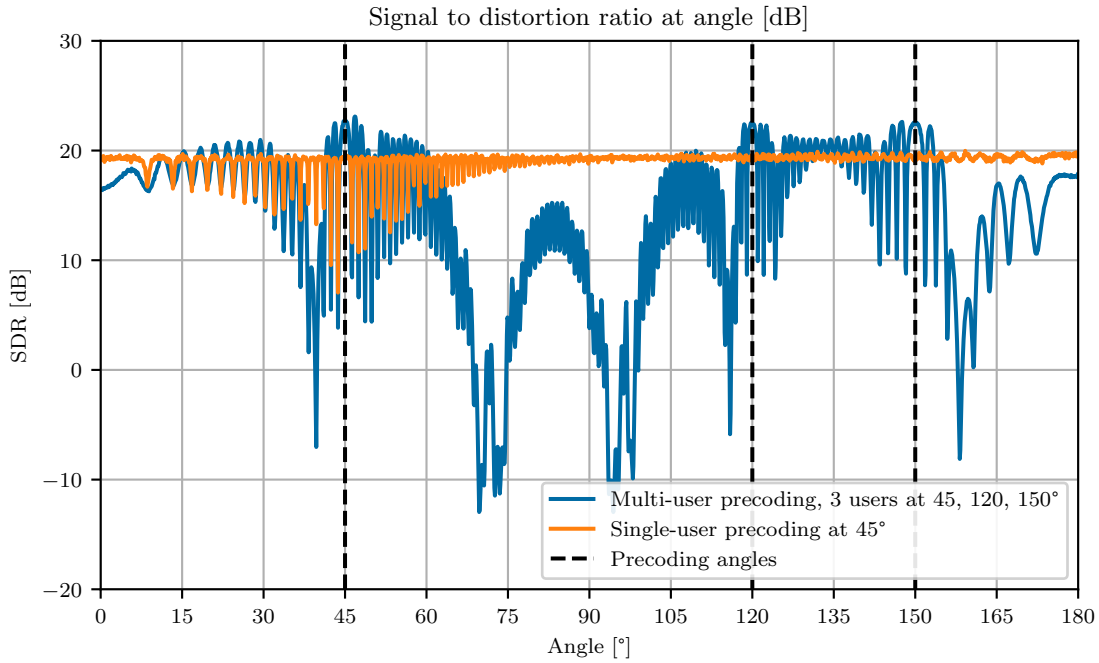

FIGURE 3.9: Signal to distortion ratio in regard to azimuth angle for multi-user precoding compared with a single-user case for two-path channel model, IBO = 3 dB and 128 antennas.

Chapter 4

Iterative receiver for M-MIMO OFDM system under front-end nonlinearities

4.1 Literature review

Addressing the problem of nonlinear distortion at the transmitter a number of PAPR reduction techniques have been proposed [17]. One commonly employed technique is Clipping And Filtering (CAF) presented in [22]. It allows for PAPR reduction without average power increase or bandwidth broadening. One critical issue of CAF is the presence of the in-band distortion originating from the clipping. In the literature two distinguished approaches toward distortion recovery, in single antenna systems, can be found: time-domain (TD) and frequency-domain (FD). The TD approach is represented by Decision-Aided Reconstruction (DAR) [19] and FD approach by Clipping Noise Cancellation (CNC) [11]. In [36] it has been shown that the CNC algorithm outperforms the DAR which was supported by derivation of theoretical performance bounds. In [32] authors propose a novel precoding method for large arrays, in which the main feature is canceling the coherent combining of the third-order nonlinear distortion. The effort and focus on the problem of the nonlinear distortion points to a conclusion that it is still of major importance even in M-MIMO systems and measures must be taken to mitigate its effects on the system's performance.

So far the M-MIMO OFDM receivers aware of nonlinear distortion have received limited attention in the literature. In [20] a neural network nonlinearity compensation for M-MIMO is presented, which can be applied both at the transmitter and receiver. The work addresses the problem by taking into consideration the distortion of the pilot signals providing channel state information. Another approach utilizing neural networks is presented in [3]. Note that the neural networks require a relatively long training period in order to characterize the nonlinearity and effectively reduce the distortion. In [1] authors analyze the performance of derived linear minimum mean squared error-based receiver for M-MIMO and nonlinearity modeled as a third-order polynomial. The receiver offers an improvement in regard to BER, however, it is still far from reaching the performance of the system without nonlinear amplification. In [12] a joint channel equalization and iterative nonlinear distortion cancellation technique is discussed in Multi-User M-MIMO scenario. The utilized algorithm is very similar to the CNC, however it was not analyzed for any type of transmit precoding. That paper was limited to Rayleigh channel model and Saleh's model of nonlinear amplification.

In this chapter, the Multi-antenna Clipping Noise Cancellation (MCNC) algorithm is proposed. Next, considering a special case of a flat fading channel a simplified version of the MCNC algorithm is presented, which has lower computational complexity and requires a lower amount of control

information. The performance of the algorithms is investigated in a single-user Massive MIMO system with MRT precoding. As shown in the previous chapter, it corresponds to the worst-case scenario when the signal-to-distortion ratio is the lowest due to the distortion being beamformed in the same direction as the desired signal. Finally, the performance and gains of the two algorithms are compared and evaluated in regard to a number of parameters.

4.2 Simple reception

In a simple receiver, first, equalization is performed, e.g., Zero Forcing (ZF), dividing received symbol r_n by $\sum_{k=1}^{K} \alpha_k h_{k,n} v_{k,n}$, effectively removing the effects of channel, precoding, and nonlinearity on wanted signal, i.e.,

$$g_n = s_n + \frac{\sum_{k=1}^{K} h_{k,n} d_{k,n}}{\sum_{k=1}^{K} \alpha_k h_{k,n} v_{k,n}} + \frac{w_n}{\sum_{k=1}^{K} \alpha_k h_{k,n} v_{k,n}}. \tag{4.1}$$

However, this results in the scaling of distortion and white noise terms.

Then the symbol detection is performed by finding the closest symbol from the constellation set:

$$\tilde{s}_n = \min_{s \in \chi} |s - g_n|^2 . \tag{4.2}$$

4.3 Multi-antenna Clipping Noise Cancellation algorithm (MCNC)

While the nonlinear distortion is often treated as white noise [7], it actually depends on the transmitted signal as shown in (2.6). Therefore, a decision-aided receiver is proposed that iteratively reproducing the received nonlinearly distorted signal improves the detection quality. While the general idea is well known for SISO OFDM systems [11], the M-MIMO precoding and utilization of multiple antennas required it to be redesigned. The Multi-antenna CNC (MCNC) receiver is shown in Fig. 4.1.

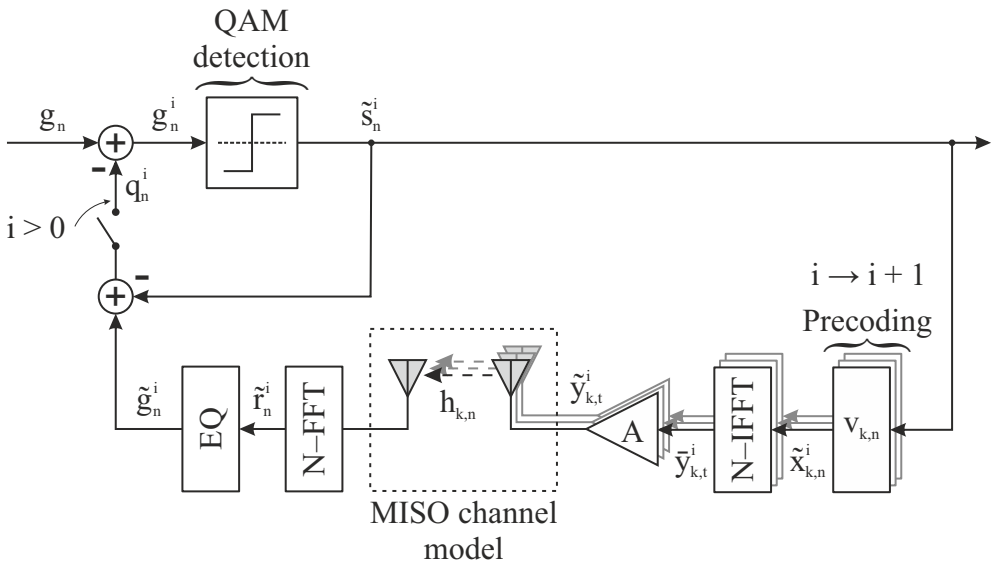

FIGURE 4.1: Multi-antenna clipping noise cancellation algorithm flowchart.

It consists of the following steps:

(a) Hard symbol detection is performed for n-th subcarrier based on the received and equalized signal g_n^i where i denotes the iteration number. For the $i = 0$ the input is the original received signal g_n as defined in (4.1). In the next iterations, the nonlinear distortion will be estimated and subtracted from g_n constituting g_n^i.

The symbol detection is carried finding the closest, from a Euclidean distance perspective, symbol from the chosen QAM constellation set χ:

$$\tilde{s}_n^i = \arg\min_{s\in\chi} \left| s - g_n^i \right|^2. \tag{4.3}$$

(b) Obtained symbol estimate $\tilde{s}_n^i$ is used to regenerate the received signal using the whole link model including a multi-antenna transmitter with nonlinear amplifiers, channel model, and receiver with equalization. To achieve this the precoding and channel coefficients need to be known at the receiver.

First, the symbol estimate is precoded as in (2.1) using the same precoding coefficients:

$$\tilde{x}_{k,n}^i = \tilde{s}_n^i v_{k,n}. \tag{4.4}$$

Then the precoded symbol estimate is OFDM modulated as in (2.4), using the same subcarrier mapping giving:

$$\bar{y}_{k,t}^i = \frac{1}{\sqrt{N}} \sum_{n\in\mathcal{N}} \tilde{x}_{k,n}^i e^{j2\pi \frac{n}{N} t}. \tag{4.5}$$

Next, the signal is processed by the nonlinearity model as in (2.5) resulting in $\tilde{y}_{k,t}^i = \mathcal{A}(\bar{y}_{k,t}^i)$. Signals obtained from each antenna are then passed through a MISO channel model similarly as in (2.14), except for white noise addition, obtaining

$$\tilde{r}_n^i = \sum_{k=1}^{K} \mathcal{F}_{[n,t=0,\ldots,N-1]}\{\tilde{y}_{k,t}^i\} h_{k,n}, \tag{4.6}$$

which is the regenerated received signal after the channel. If all the symbols $\tilde{s}_n^i$ are correct both the wanted signal and nonlinear distortion will be perfectly reconstructed. While this is not probable under severe nonlinearity or noise if most of the symbols $\tilde{s}_n^i$ are detected correctly the majority of nonlinear distortion should be reconstructed as well [11].

The regenerated signal can be decomposed into desired and distortion components based on (2.9) as:

$$\tilde{r}_n^i = \sum_{k=1}^{K} \alpha_k h_{k,n} v_{k,n} \tilde{s}_n^i + \sum_{k=1}^{K} h_{k,n} \tilde{d}_{k,n}^i, \tag{4.7}$$

where $\tilde{d}_{k,n}^i$ denotes the reconstructed distortion signal received from k-th antenna on n-th subcarrier in i-th iteration. The regenerated signal undergoes equalization by dividing the signal by $\sum_{k=1}^{K} \alpha_k h_{k,n} v_{k,n}$ giving

$$\begin{aligned} \tilde{g}_n^i &= \frac{\tilde{r}_n^i}{\sum_{k=1}^{K} \alpha_k h_{k,n} v_{k,n}} \\ &= \tilde{s}_n^i + \frac{\sum_{k=1}^{K} h_{k,n} \tilde{d}_{k,n}^i}{\sum_{k=1}^{K} \alpha_k h_{k,n} v_{k,n}}. \end{aligned} \tag{4.8}$$

The last component in (4.8) is nonlinear distortion influencing n-th subcarrier if symbols $\tilde{s}_n^i$ were transmitted. While both g_n^i and $\tilde{s}_n^i$ are known at this stage this signal can be calculated as

$$q_n^i = \tilde{g}_n^i - \tilde{s}_n^i. \tag{4.9}$$

(c) The estimated distortion component is subtracted from the originally received signal

$$g_n^{i+1} = g_n - q_n^i \tag{4.10}$$

constructing potentially improved received signal that can be used for detection in the next iteration. The algorithm returns to step (a) and repeats until a certain number of iterations has been reached or satisfactory quality of the received data has been achieved.

Using (4.1) and (4.8) the components of g_n^{i+1} can be shown as:

$$g_n^{i+1} = s_n + \frac{\sum_{k=1}^{K} h_{k,n}\left(d_{k,n} - \tilde{d}_{k,n}^i\right) + w_n}{\sum_{k=1}^{K} \alpha_k h_{k,n} v_{k,n}}. \tag{4.11}$$

If the $\tilde{s}_n^i$ estimates are good enough, the estimated nonlinear distortion term $\tilde{d}_{k,n}^i$ should reduce the received distortion term $d_{k,n}$ improving the reception performance.

One of the disadvantages of the above algorithm is the requirement to know the channel coefficients and the precoding vectors used at the transmitter. This can be difficult to be obtained in Time Division Duplex (TDD)-based Massive MIMO system in which channel reciprocity property is used [23]. In such a case transmission of channel coefficients $h_{k,n}$ together with the utilized precoding coefficients $v_{k,n}$ will require a significant capacity of the control channel, especially for a high number of antennas and a frequency selective channel.

4.4 Clipping Noise Cancellation algorithm (CNC)

Considering the above-mentioned drawbacks of MCNC a reasonable is to propose a simplification resulting in lower computational complexity and a lower amount of control information required in the receiver.

An example to start with is a precoder being fixed for all subcarriers of a given antenna. Moreover, equal precoder amplitude for each antenna is assumed that, considering (2.2), results in $|v_{k,n}| = \frac{1}{\sqrt{K}}$. Therefore, the precoding coefficient equals

$$v_{k,n} = \frac{1}{\sqrt{K}} e^{j\varphi_k}, \tag{4.12}$$

where φ_k is precoder phase shift specific for the k-th antenna. This allows us to simplify (2.4) as follows:

$$y_{k,t} = \frac{1}{\sqrt{K}} e^{j\varphi_k} \underbrace{\frac{1}{\sqrt{N}} \sum_{n\in\mathcal{N}} s_n e^{j2\pi \frac{n}{N} t}}_{\ddot{y}_t}. \tag{4.13}$$

By combining (2.8) and (2.7) the clipping power of the considered PA can be defined as

$$P_{\max} = 10^{\frac{\mathrm{IBO}}{10}} \frac{\bar{P}_s N_{\mathrm{u}}}{KN}. \tag{4.14}$$

The precoded signal after the nonlinearity (2.6) can be rewritten as:

$$\hat{y}_{k,t} = \begin{cases} \frac{1}{\sqrt{K}} e^{j\varphi_k} \ddot{y}_t & \text{for } \left|\frac{1}{\sqrt{K}} \ddot{y}_t\right|^2 \leq P_{\max} \\ \sqrt{P_{\max}} e^{j\varphi_k + j \arg(\ddot{y}_t)} & \text{for } \left|\frac{1}{\sqrt{K}} \ddot{y}_t\right|^2 > P_{\max} \end{cases}. \tag{4.15}$$

This can be reformulated by taking the precoding coefficient as a common multiplier giving:

$$\hat{y}_{k,t} = \frac{1}{\sqrt{K}} e^{j\varphi_k} \begin{cases} \ddot{y}_t & \text{for } |\ddot{y}_t|^2 \leq \ddot{P}_{\max} \\ \sqrt{\ddot{P}_{\max}} e^{j \arg(\ddot{y}_t)} & \text{for } |\ddot{y}_t|^2 > \ddot{P}_{\max} \end{cases}, \tag{4.16}$$

where $\ddot{P}_{\max} = 10^{\frac{\mathrm{IBO}}{10}} \frac{\bar{P}_s N_{\mathrm{u}}}{N}$ is clipping power for $K = 1$ antenna. The last formula shows that for the considered precoder the signal at k-th antenna can be obtained by passing OFDM symbols obtained without precoding through a single PA (of the same IBO parameter) and scaling the PA output by the precoding coefficient before transmission through the antenna. In other words, the considered amplifier can be treated as a linear operator for the precoding coefficient. Both the wanted signal and distortion as decomposed in (2.15) are only linearly scaled by the precoding coefficient. Similarly as in (2.9) the input to k-th antenna at time instance t can be decomposed as:

$$\hat{y}_{k,t} = \frac{1}{\sqrt{K}} e^{j\varphi_k} \left(\alpha \ddot{y}_t + \ddot{\ddot{d}}_t\right), \tag{4.17}$$

where $\ddot{\ddot{d}}_t$ is distortion sample at time instance t. Observe it is independent of the precoding and the antenna index. Most interestingly, α is equal for each antenna and is the same as if precoding is considered before IFFT as in the MCNC algorithm. This is the result of α being dependent only on the IBO value as shown in (2.13). Following the same reasoning as in Sec. 2.1 the received signal at n-th subcarrier is obtained:

$$r_n = \alpha s_n \frac{1}{\sqrt{K}} \sum_{k=1}^{K} e^{j\varphi_k} h_{k,n} + \ddot{d}_n \frac{1}{\sqrt{K}} \sum_{k=1}^{K} e^{j\varphi_k} h_{k,n} + w_n, \tag{4.18}$$

where

$$\ddot{d}_n = \mathcal{F}_{[n,t=0,\ldots,N-1]} \left\{\ddot{\ddot{d}}_t\right\}. \tag{4.19}$$

Initial ZF equalization results in

$$g_n = s_n + \frac{\ddot{d}_n}{\alpha} + \frac{w_n}{\frac{\alpha}{\sqrt{K}} \sum_{k=1}^{K} e^{j\varphi_k} h_{k,n}}. \tag{4.20}$$

While the aim of the proposed reception method is to reconstruct the clipping noise (distortion) this becomes relatively simple in this case. The values of $\ddot{d}_n$ depend only on the transmitted symbols s_n and the PA IBO value. There is no need to know the channel coefficients and precoders nor to reconstruct all K transmission chains.

This allows us to propose a CNC algorithm for simplified reconstruction of clipping noise in M-MIMO system, that has a similar structure as the algorithm described [36] for single antenna systems. The signal processing flowchart of the CNC algorithm is shown in Fig. 4.2. Its iterative structure is similar to the one used by MCNC except for using channel and precoding coefficients and multiple transmit antennas. The proposed CNC algorithm is derived using a very specific precoding case. However, as will be supported by simulation results, it can be used for more realistic precoding conditions as well, providing only slight performance degradation in comparison to the MCNC algorithm.

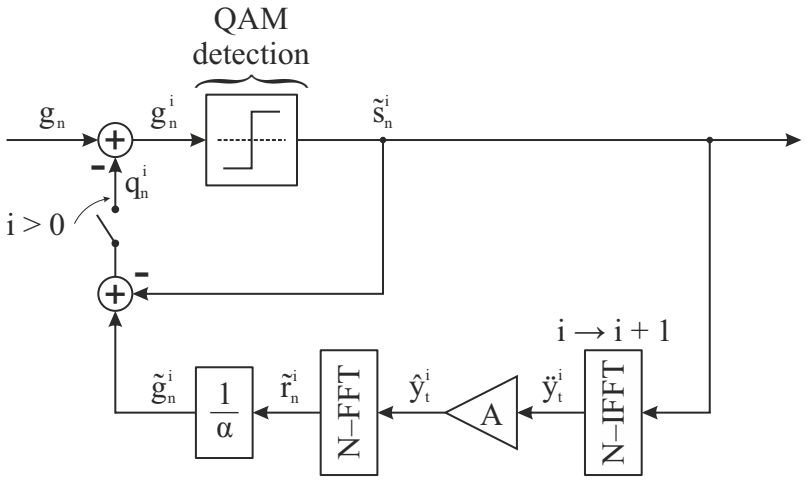

FIGURE 4.2: Clipping Noise Cancellation algorithm flowchart.

4.5 Computational complexity

In this section, the computational complexity of a standard OFDM receiver, CNC and MCNC algorithms is analyzed. The FFT and IFFT is performed by radix-2 algorithm and requires $(N/2)\log_2 N$ complex multiplications and $N\log_2 N$ complex additions [30]. Each complex multiplication can be split into 3 real multiplications and 5 additions [9] and each complex addition can be treated as two real additions. With these simplifications the FFT/IFFT operation cost is: $3\left((N/2)\log_2 N\right)$ real multiplications and $5\left((N/2)\log_2 N\right) + 2N\log_2 N$ real additions.

A single QAM symbol detection based on Euclidean distance (4.2) requires M comparisons, $2M$ real multiplications and $3M$ real additions, where M is the constellation size. The OFDM symbol detection requires then $N_{\mathrm{U}}(M)$ comparisons, $2N_{\mathrm{U}}M$ real multiplications and $3N_{\mathrm{U}}M$ real additions. The precoding for a single front-end in a single-user case requires $\mathrm{N_U}$ complex multiplications, which translates for $3N_{\mathrm{U}}$ real multiplications and $5N_{\mathrm{U}}$ additions. A similar number of operations is required by the equalization and SISO channel propagation. Division by α coefficient requires two real divisions for each sample in N_{U} vector.

Processing by a single nonlinear front-end requires N comparisons, 2N multiplications, N additions. When the sample power exceeds the threshold it is multiplied by the square root of saturation power divided by the sample power. The CORDIC algorithm is employed to calculate the square root, which according to [24] requires 1 table lookup, 2 shifts, 3 real additions per iteration for a fixed point approximation. The number of iterations depends on the desired precision of the result, with each iteration corresponding to a single bit. Assuming the use of single precision floating arithmetic the number of iterations required by CORDIC is set to 23 [29], resulting in 23 table lookups 46 shifts, 69 real additions. This adds 2N real multiplications, N divisions and 69N additions to the complexity of the operation. In the following algorithm complexity analysis, only the additions/subtractions and multiplication/divisions are taken into consideration. Table 4.1 presents a summarized number of operations for each signal processing step.

Computational complexity of considered receivers:

- Standard OFDM receiver: consisting of equalization, FFT and detection:
  Number of additions/subtractions:

$$5N_{\mathrm{U}} + 5((N/2)\log_2 N) + 2N\log_2 N + 3N_{\mathrm{U}}M \tag{4.21}$$

TABLE 4.1: Number of operations of selected signal processing steps.

Signal processing step	Operation count	
	Additions/Subtractions	Multiplications/Divisions
OFDM symbol detection	$3N_{\mathrm{U}}M$	$2N_{\mathrm{U}}M$
FFT/IFFT	$5\left((N/2)\log_2 N\right) + 2N\log_2 N$	$3\left((N/2)\log_2 N\right)$
Equalization	$5N_{\mathrm{U}}$	$3N_{\mathrm{U}}$
SISO Precoding	$5N_{\mathrm{U}}$	$3N_{\mathrm{U}}$
SISO Propagation	$5N_{\mathrm{U}}$	$3N_{\mathrm{U}}$
SISO Nonlinearity	$70N$	$5N$

Number of multiplications/divisions:

$$3N_{\mathrm{U}} + 3((N/2)\log_2 N) + 2N_{\mathrm{U}}M \tag{4.22}$$

- Clipping Noise Cancellation (CNC) receiver:
  Number of additions/subtractions:

$$\begin{aligned}&\underbrace{5N_{\mathrm{U}} + 5((N/2)\log_2 N) + 2N\log_2 N + 3N_{\mathrm{U}}M}_{\text{0-th iteration}}\\&+ I\Big(2\big(5((N/2)\log_2 N) + 2N\log_2 N\big) + 70N + 2N_{\mathrm{U}} + 3N_{\mathrm{U}}M\Big)\end{aligned} \tag{4.23}$$

  Number of multiplications/divisions:

$$\begin{aligned}&\underbrace{3N_{\mathrm{U}} + 3((N/2)\log_2 N) + 2N_{\mathrm{U}}M}_{\text{0-th iteration}}\\&+ I\Big(2\big(3((N/2)\log_2 N)\big) + 5N + 2N_{\mathrm{U}} + 2N_{\mathrm{U}}M\Big)\end{aligned} \tag{4.24}$$

- Multi-antenna Clipping Noise Cancellation (MCNC) receiver:
  Number of additions/subtractions:

$$\begin{aligned}&\underbrace{5N_{\mathrm{U}} + 5((N/2)\log_2 N) + 2N\log_2 N + 3N_{\mathrm{U}}M}_{\text{0-th iteration}}\\&+ I\Big((K+1)\big(5((N/2)\log_2 N) + 2N\log_2 N\big) + 70KN + (2K+1)(5N_{\mathrm{U}})\\&+ (K-1) + 2N_{\mathrm{U}} + 3N_{\mathrm{U}}M\Big)\end{aligned} \tag{4.25}$$

  Number of multiplications/divisions:

$$\begin{aligned}&\underbrace{3N_{\mathrm{U}} + 3((N/2)\log_2 N) + 2N_{\mathrm{U}}M}_{\text{0-th iteration}}\\&+ I\Big((K+1)\big(3((N/2)\log_2 N)\big) + 5KN + (2K+1)3N_{\mathrm{U}} + 2N_{\mathrm{U}}M\Big)\end{aligned} \tag{4.26}$$

Table 4.2 presents the total number of arithmetic operations required for each iteration of the CNC and MCNC algorithm for $M = 64, N = 4096, N_{\mathrm{U}} = 2048, K = 64$ and a selected number of iterations. The values presented for the 0-th iteration correspond to the standard receiver, which performs equalization and demodulation. It can be seen that the complexity of the MCNC algorithm grows rapidly with the number of iterations and is substantially higher due to individual signal processing for each of the transmit antennas in the system. On the other hand, CNC algorithm complexity is relatively close to the standard receiver, which may advocate its application.

TABLE 4.2: Total number of operations for $M = 64, N = 4096, N_{\mathrm{U}} = 2048, K = 64$, and a selected number of iterations of the CNC and MCNC algorithms.

Number of iterations: I	Total number of operations (10^6)			
	Additions/subtractions		Multiplications/divisions	
	CNC	MCNC	CNC	MCNC
0	0.62	0.62	0.34	0.34
1	1.75	35.07	0.78	7.50
2	2.88	69.52	1.21	14.66
3	4.00	103.96	1.64	21.82
4	5.13	138.41	2.08	28.97
5	6.26	172.85	2.51	36.13
6	7.38	207.30	2.95	43.29
7	8.51	241.74	3.38	50.45
8	9.64	276.19	3.82	57.60

4.6 Simulation results

To evaluate the performance of considered clipping noise cancellation algorithms a numerical simulation was performed. The key parameters of the simulator remain the same as presented in Sec. 2.2. Each result was obtained after transmitting approximately 800 OFDM symbols with independent modulating symbols. For the Rayleigh channel, each OFDM symbol was transmitted through an independently generated channel. For the LOS and two-path channels for each OFDM symbol, the position of the receiver was picked randomly within a 10m square centered at the reference position.

In order to present gains from MCNC and CNC methods, the IBO is set 0 dB (significant nonlinear distortion), K to 64 and BER was measured for varying Eb/N0 and a number of RX iterations. The results for LOS, two-path and Rayleigh channels are presented in Fig. 4.3, 4.4, and 4.5, respectively.

First, it is visible that results for LOS and two-path channels are very close to each other in all considered scenarios, revealing significant distortions level resulting in BER close to 10^{-1} for a standard receiver in the whole observation range. This shows, similarly to Fig. 3.6, that not only LOS channel, as shown in [21], but also a sparse multi-path channel can suffer from nonlinear distortion in M-MIMO systems. Observe that in the case of the Rayleigh channel the directly received distorted signal (0th iteration) achieves much lower BER for the same Eb/N0 in relation to LOS or a two-path channel. This is the result of antenna array gain improving SDR as has been shown in Fig. 3.6. Secondly, for all considered channels MCNC allows to achieve the BER limit observed for a system without nonlinear distortion (*No dist* in figures) after no more than 8 iterations. The BER improvement increases with the number of RX iterations. However, this happens at the cost of significant computational complexity as the receiver has to emulate signal processing of all considered TX-RX links. In an example, the CNC algorithm requires 8 iterations to achieve BER of 10^{-3} for Eb/N0 equal to 16 dB. Meanwhile, the MCNC algorithm achieves the same BER given the same Eb/N0 using only 5 iterations. However, the cost of 8 iterations of CNC is 9.64 million of additions/subtractions and 3.82 million of multiplications/divisions compared to 172.85 and 36.13 million of respective operations for 5 iterations of MCNC.

Significantly, lower computational complexity and a lower amount of control information are required by the CNC algorithm. As visible in Fig. 4.3, and Fig. 4.4 the CNC algorithm allows for significantly improved BER for LOS and two-path channels. However, the performance is slightly

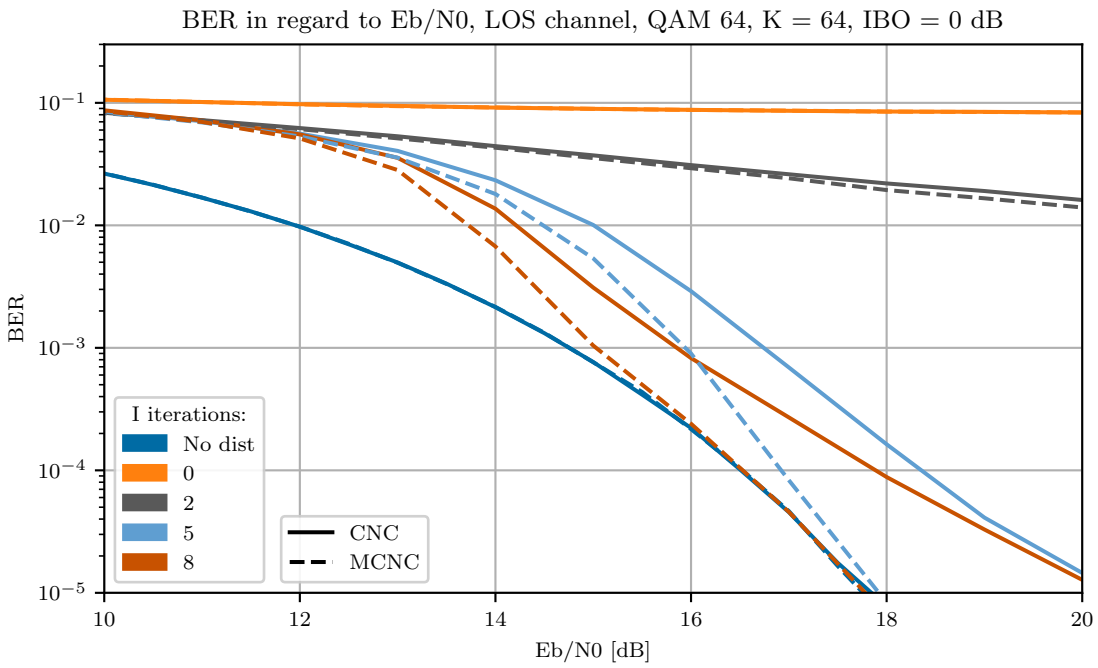

FIGURE 4.3: BER in regard to Eb/N0 for IBO = 0 dB, for K = 64 antennas, LOS channel and a selected number of iterations of the CNC and MCNC algorithms.

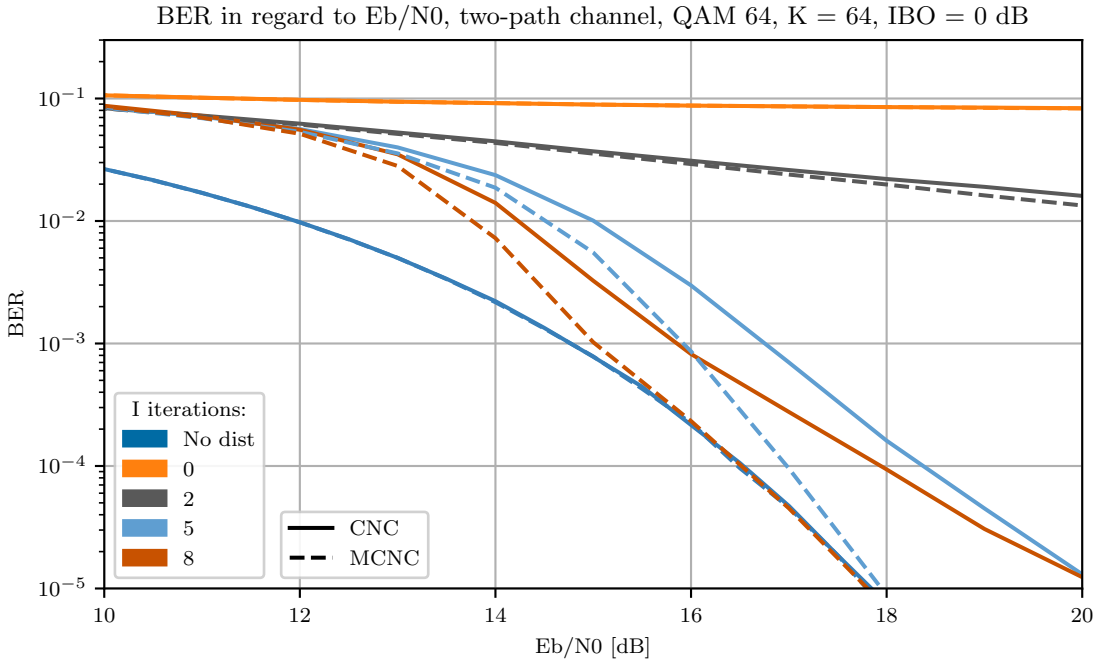

FIGURE 4.4: BER in regard to Eb/N0 for IBO = 0 dB, for K = 64 antennas, two-path channel and a selected number of iterations of the CNC and MCNC algorithms.

worse than that of the MCNC algorithm. After the 8th iteration for BER= 10^{-5} the loss equals about 2 dB in Eb/N0. On the other hand, for the considered Rayleigh channel the utilization of the CNC algorithm increases BER. While there is an independent random channel coefficient on each subcarrier for each TX antenna, the MRT precoding coefficient varies similarly influencing samples of nonlinear distortion, i.e., $\sum_{k=1}^{K} h_{k,n} d_{k,n}$ in (2.17). While the CNC algorithm is unaware of the precoding it is reconstructing the clipping noise that is significantly different than the real

one's deteriorating reception performance.

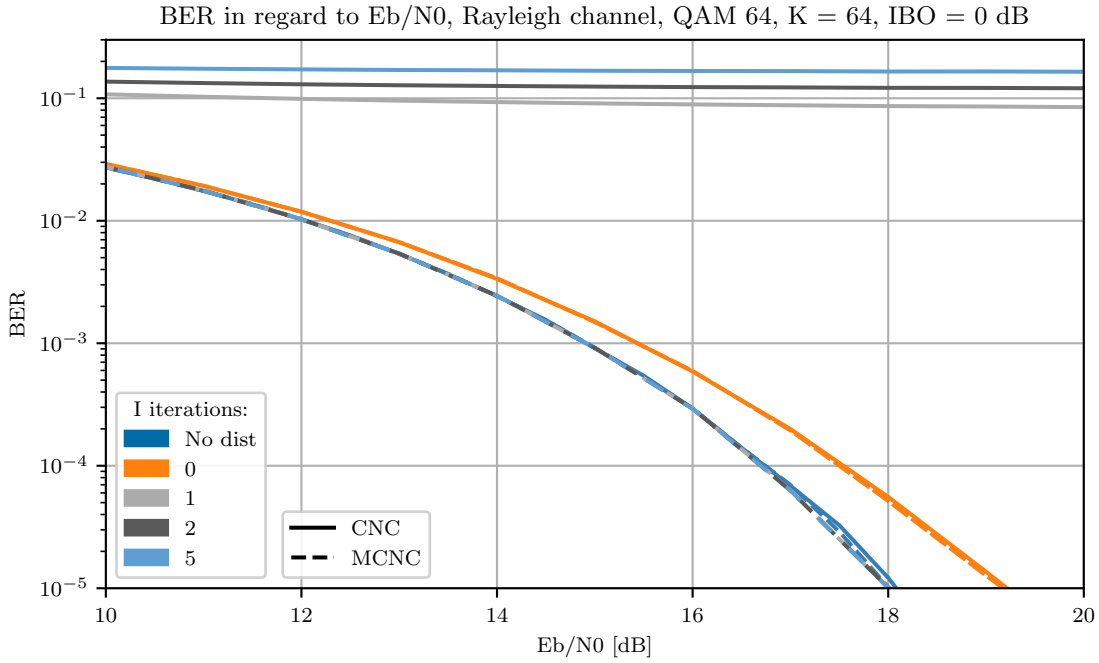

FIGURE 4.5: BER in regard to Eb/N0 for IBO = 0 dB, for K = 64 antennas, Rayleigh channel and a selected number of iterations of the CNC and MCNC algorithms.

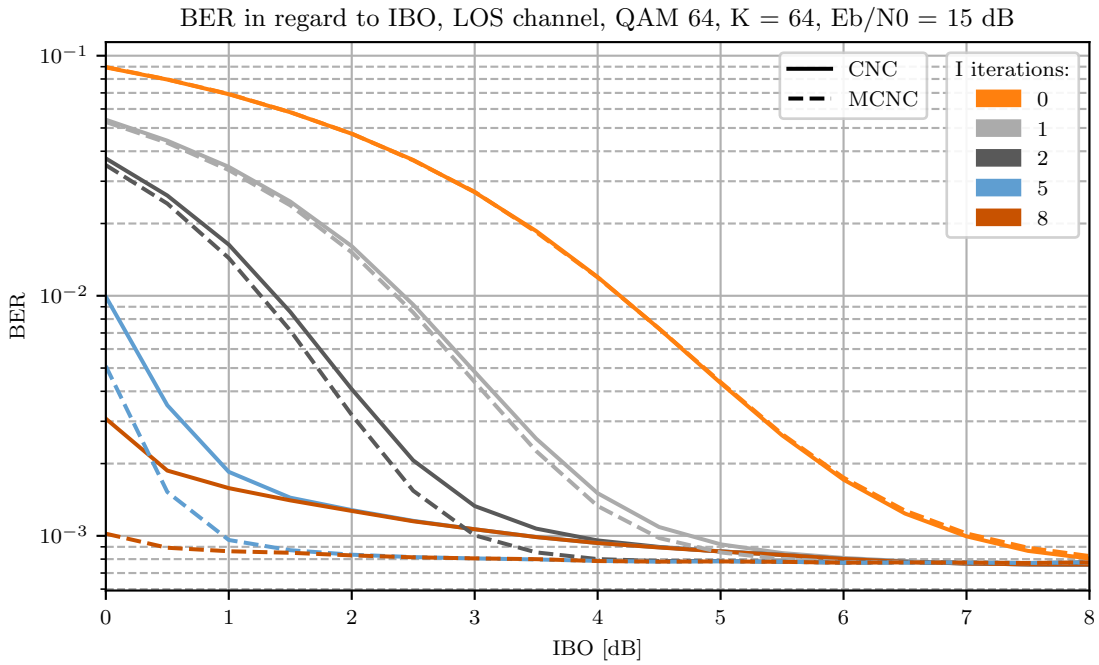

FIGURE 4.6: BER in regard to IBO for Eb/N0 = 15 dB, K = 64 antennas, LOS channel and a selected number of iterations of the CNC and MCNC algorithms.

Next, the proposed RX algorithms are tested for varying PA operating points, i.e., IBO. The Eb/N0 is fixed to 15 dB and the number of antennas is K=64. BER curves for LOS, two-path and Rayleigh channels are shown in Fig. 4.6, 4.7, and Fig. 4.8, respectively. The figures for LOS channel are once again nearly identical as for the two-path channel. The results confirm the previous observations. The MCNC algorithm achieves a noise-limited BER floor around 10^{-3}

after a sufficiently high number of iterations. The lower the clipping level the more iterations are needed. The CNC algorithm provides BER improvement with respect to the standard receiver (0th iteration) only for two-ray and LOS channels being slightly outperformed by the MCNC algorithm.

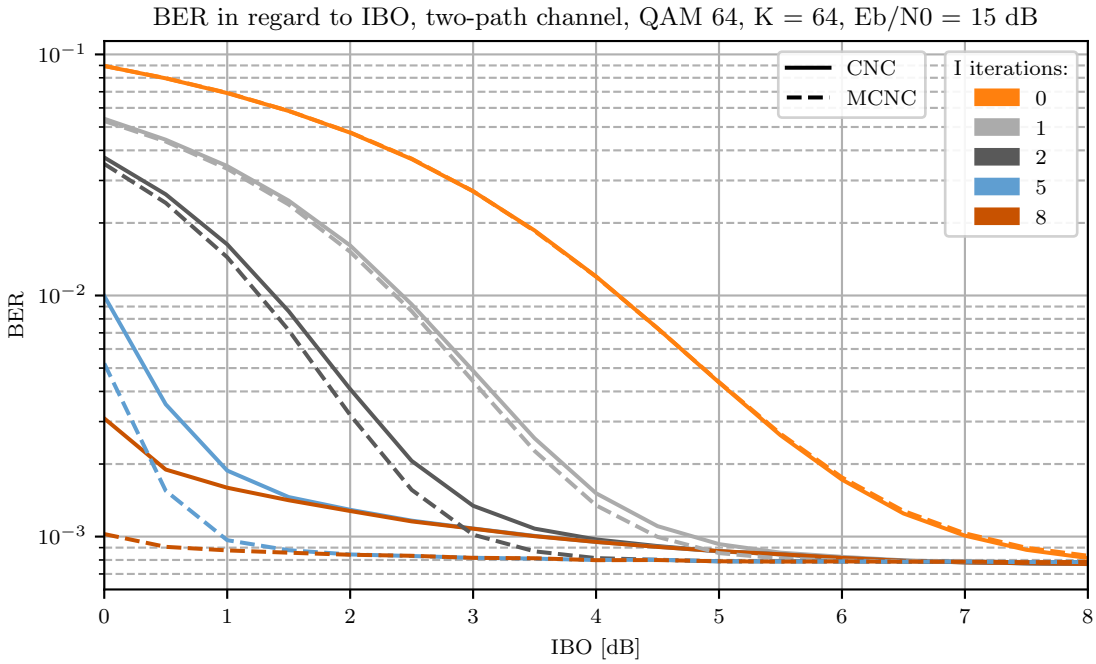

FIGURE 4.7: BER in regard to IBO for Eb/N0 = 15 dB, K = 64 antennas, two-path channel and a selected number of iterations of the CNC and MCNC algorithms.

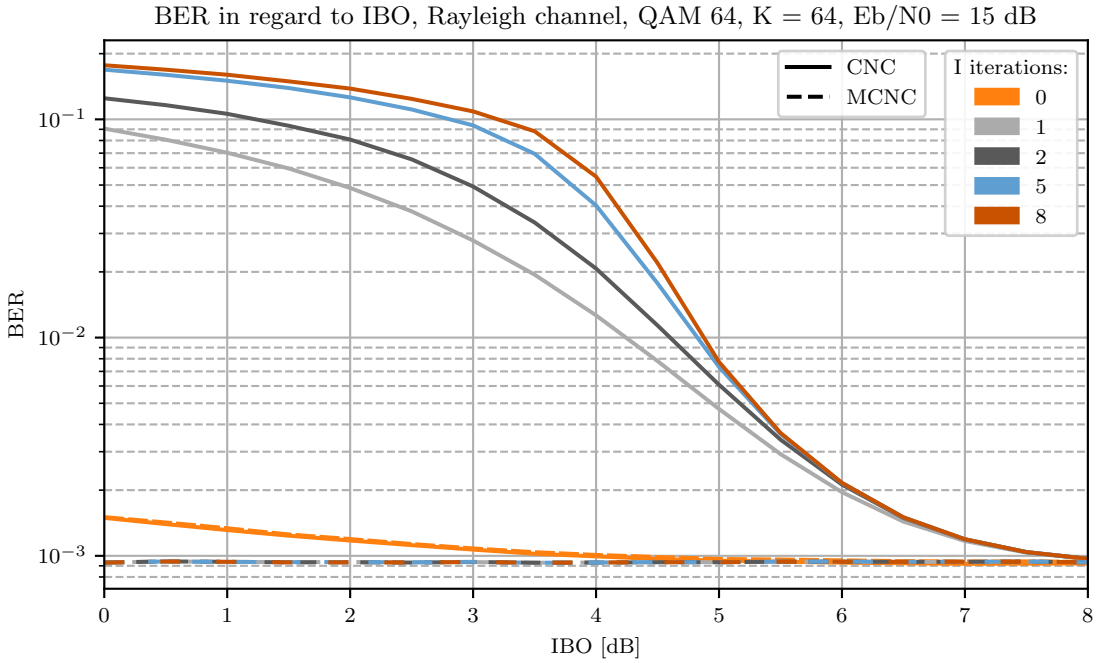

FIGURE 4.8: BER in regard to IBO for Eb/N0 = 15 dB, K = 64 antennas, Rayleigh channel and a selected number of iterations of the CNC and MCNC algorithms.

Figure 4.9, 4.10 and 4.11 visualize the gains of the CNC and MCNC algorithm for a fixed BER value equal to 10^{-2} in regard to both Eb/N0 and IBO. This form of presentation allows to evaluate the gains from using a specific number of iterations. Given the IBO it is possible to estimate the

margin by which the Eb/N0 requirements can be reduced for a certain number of iterations and vice versa. For direct visibility channels: LOS and two-path the results are highly identical and differ only in terms of simulation accuracy. In Fig. 4.9 and 4.10 it can be observed that for those channels the gains from using MCNC algorithm over standard CNC become apparent since the second iteration. The lower the IBO the higher number of iterations is required to meet the Eb/N0 12 dB floor which corresponds to the system without nonlinear distortion. For the Rayleigh

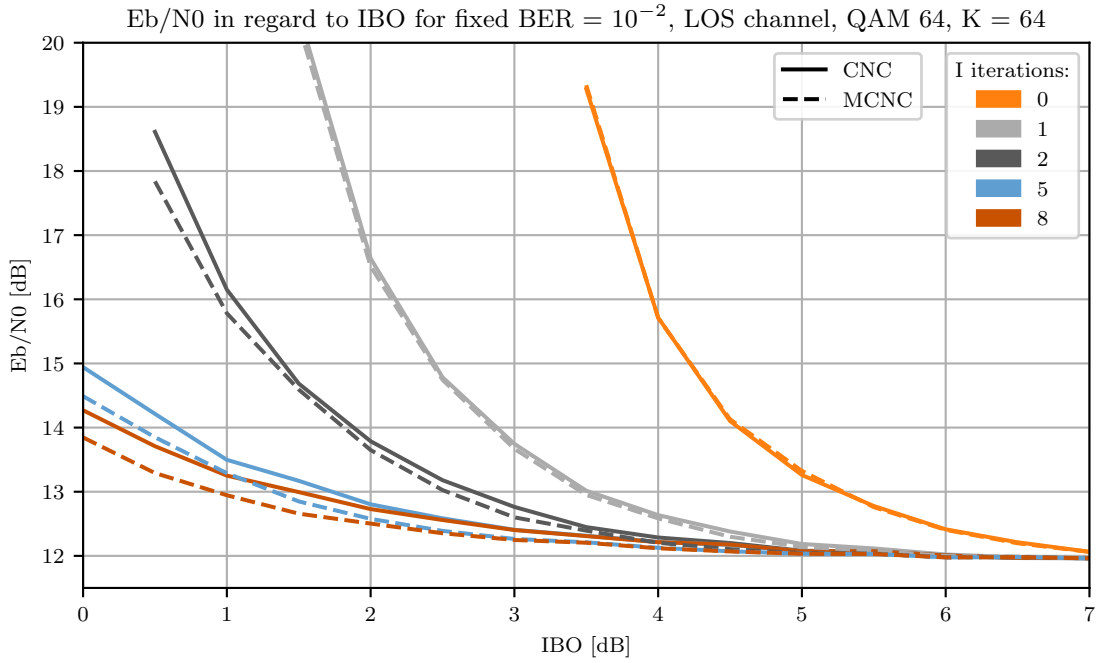

FIGURE 4.9: Eb/N0 in regard to IBO for a fixed BER = 10^{-2}, 64 antennas, LOS channel and a selected number of iterations of the CNC and MCNC algorithms.

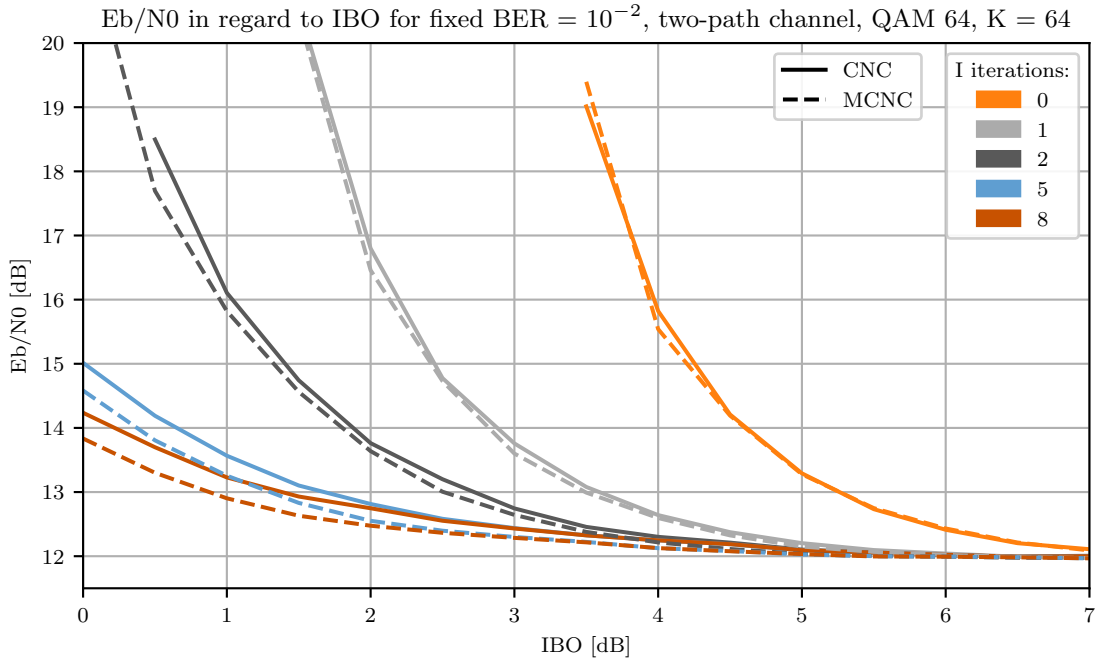

FIGURE 4.10: Eb/N0 in regard to IBO for a fixed BER = 10^{-2}, 64 antennas, two-path channel and a selected number of iterations of the CNC and MCNC algorithms.

channel and MCNC reception in Fig. 4.11 required Eb/N0 curve is almost flat for any value of IBO from the range . The first iteration of the MCNC offers minimal improvement. This is due to a high number of antennas $K = 64$, which translates into higher SDR in Rayleigh channel than as could be seen in Fig. 3.6, lessening the severity of impact of nonlinear distortion on the received signal and allowing the algorithm to work with less nonlinear distortion interference.

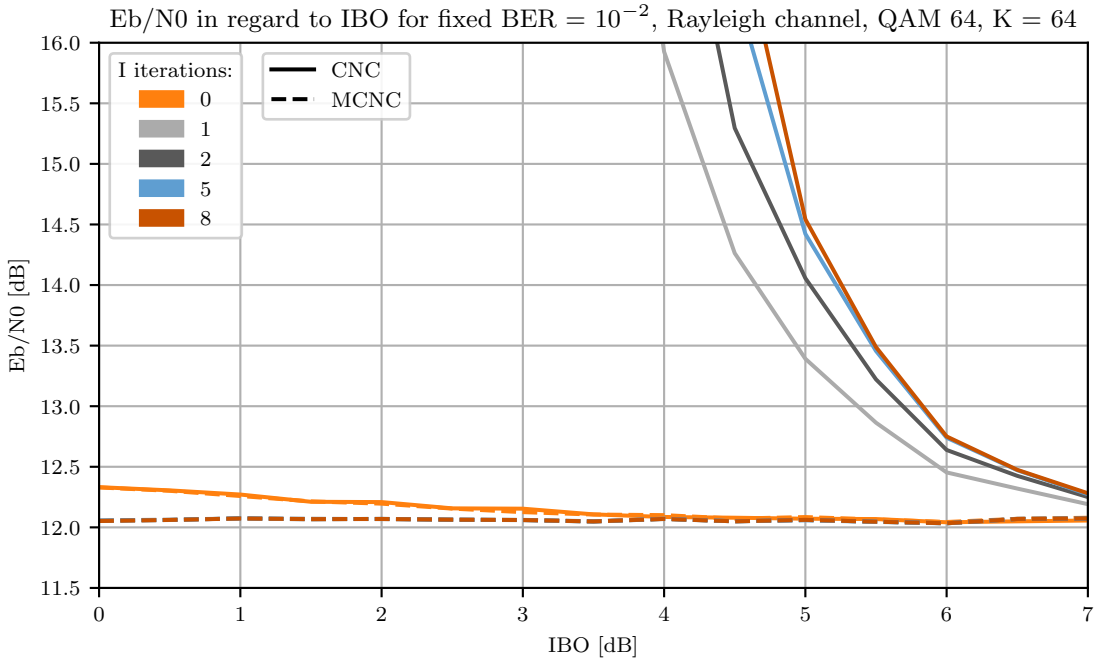

FIGURE 4.11: Eb/N0 in regard to IBO for a fixed BER = 10^{-2}, 64 antennas, Rayleigh channel and a selected number of iterations of the CNC and MCNC algorithms.

Figure 4.12 presents a comparison between CNC and MCNC algorithms taking into consideration the channel kind, number of RX iterations, and number of antennas K. The first observation can be a significant decrease of BER for the Rayleigh channel with a number of antennas. This effect is caused by averaging of the channel resulting in higher signal power at the receiver and lower noise amplification during equalization. As expected from previous results, while the MCNC helps to improve the BER performance, the CNC algorithm increases BER in this scenario. For a high number of antennas in the Rayleigh channel, the SDR gains allow the MCNC algorithm to quickly converge within a single iteration to the noise-limited bound denoted as *No dist.* On the other hand, the CNC algorithm works well for LOS and two-path channels achieving BER slightly higher than the MCNC algorithm. Again, the performance of LOS and two-path channels is nearly identical. An interesting observation for these channels is that while the BER performance for both RX algorithms remains constant up to about K=16 antennas it starts to slightly decrease for higher K and higher number of RX iterations.

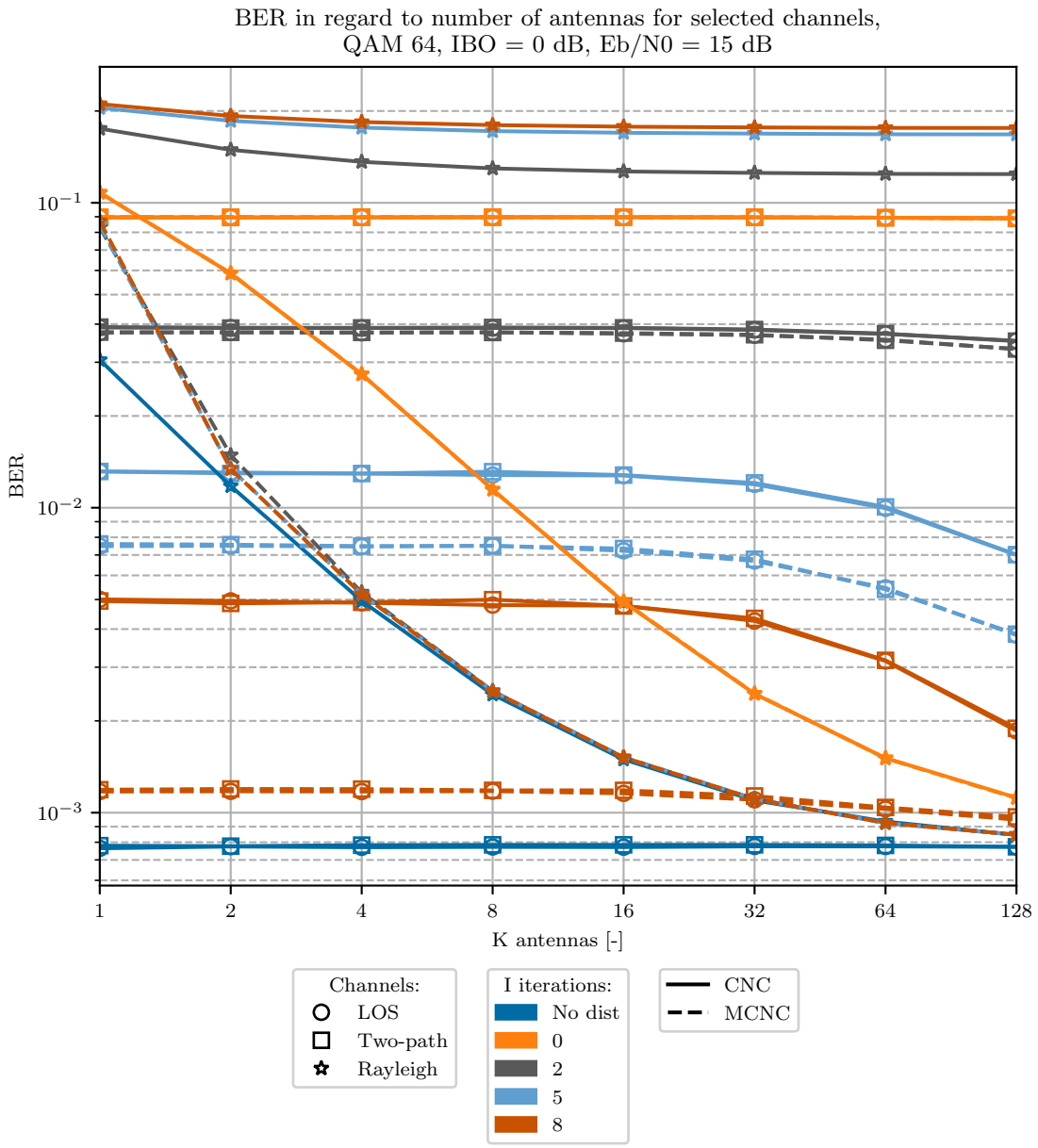

FIGURE 4.12: BER in regard to the number of antennas, and channels for Eb/N0 = 15 dB, IBO = 0 dB, and a selected number of iterations of the CNC and MCNC algorithms.

The results presented up to this point have shown limited gains from using greater than one number of iterations of the MCNC algorithm for systems with a high number of antennas and Rayleigh channel. The algorithm quickly converges to the performance bound even for low IBO values due to SDR scaling with a number of antennas for the Rayleigh channel, which was discussed in Sec. 3.2. The gains from subsequent iterations of the MCNC are more visible when investigating a single antenna system performance in Rayleigh channel. The receiver is then exposed to the same levels of signal-to-distortion levels as in LOS or two-path channels. Figure 4.13 presents the BER performance of the algorithms in regard to Eb/N0. The plot shows that each iteration of the MCNC algorithm provides a gain in terms of BER performance for high values of Eb/N0. The CNC algorithm iterations worsen the performance as they do take into account the effects of precoding on the received signal. Notice how for the Rayleigh SISO case the algorithm starts to recover and remove the nonlinear distortion effectively starting from the Eb/N0 of about 16 dB.

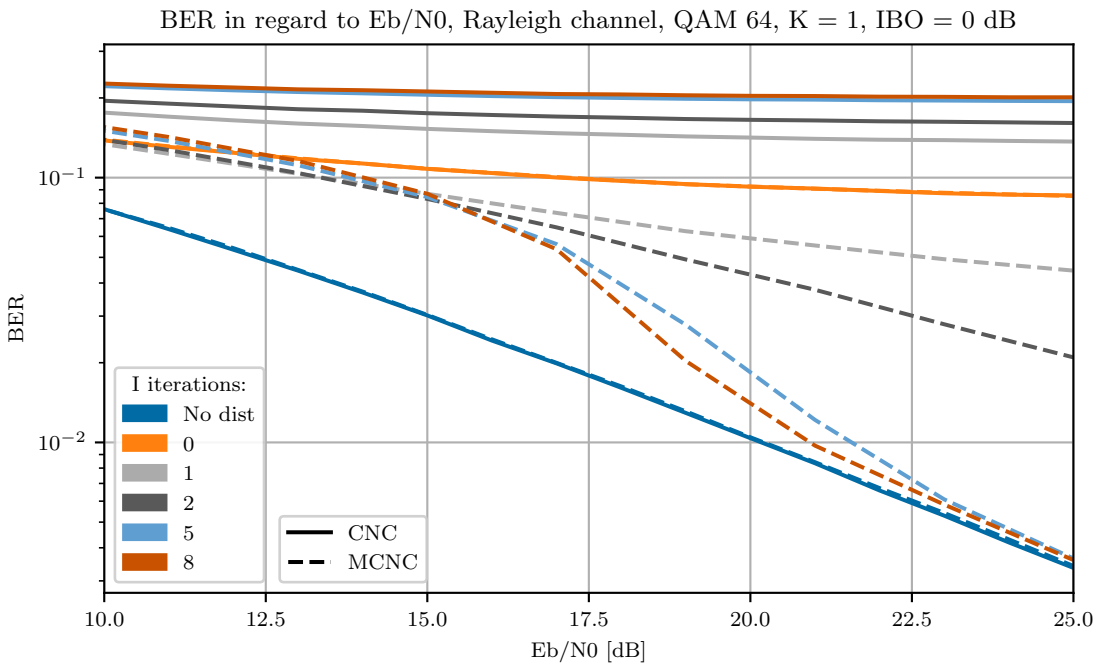

FIGURE 4.13: BER in regard to Eb/N0 for IBO = 0 dB, for K=1 antenna, Rayleigh channel and a selected number of iterations of the CNC and MCNC algorithms.

Figure 4.14 presents the BER performance for a fixed value of Eb/N0 and varying IBO for SISO system and Rayleigh channel. From the plot, it can be read that increasing the number of iterations from 1 to 2 of the MCNC algorithm allows to reduce the IBO requirements for a given BER by about 1 dB, which is a relatively large value. Once again it can be observed that each iteration of the MCNC algorithm offers improvement in regard to BER for low IBO values.

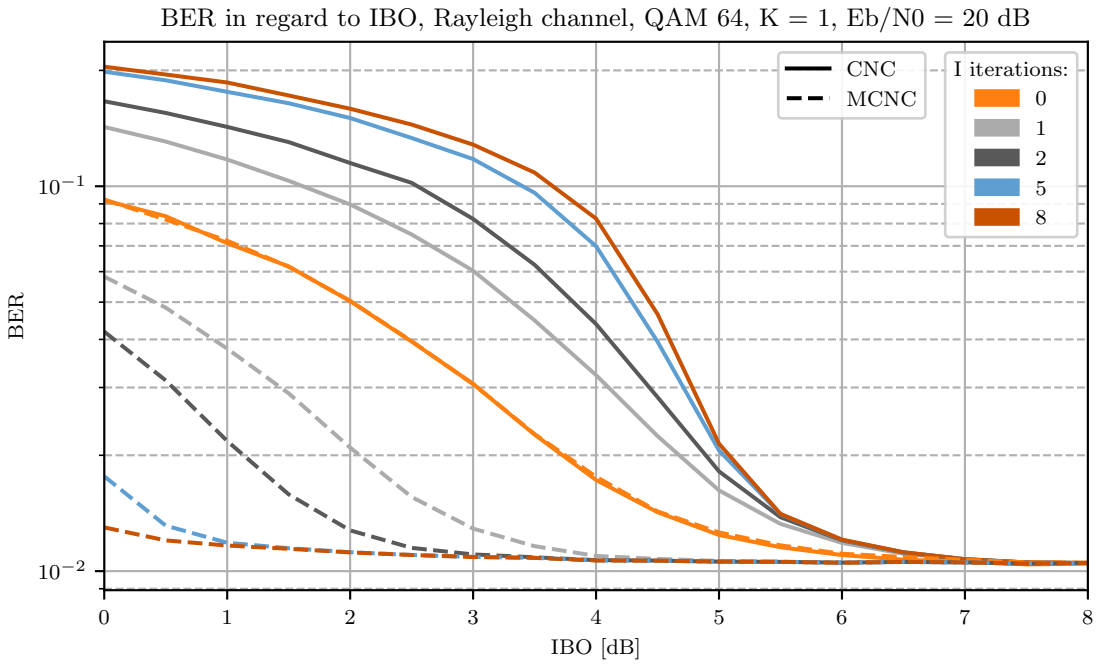

FIGURE 4.14: BER in regard to IBO for Eb/N0 = 20 dB, K = 1 antenna, Rayleigh channel and a selected number of iterations of the CNC and MCNC algorithms.

Figure 4.15 visualizes the gains of the algorithms for a target value of BER of 10^{-2} in regard

to Eb/N0 and IBO. Based on the plot it is possible to estimate the value by which IBO or Eb/N0 requirements can be reduced for each iteration. For example, increasing the number of iterations from 1 to 2 allows to reduce the IBO requirements by approximately 1 dB or reduce the Eb/N0 requirement by about 1.5 dB for IBO equal to 2.5 dB, guaranteeing the same BER performance. Similarly, as in previous analyses, the subsequent CNC algorithm iterations only worsen the performance of the system and increase the requirements instead of decreasing them.

The analysis of the MCNC in SISO Rayleigh channel allows to present a new use-case of the algorithm, proving that its application is not limited to MIMO systems. To some extent, this analysis can be compared with the multi-antenna scenarios as it provides results for the same SDR value as in direct visibility channels.

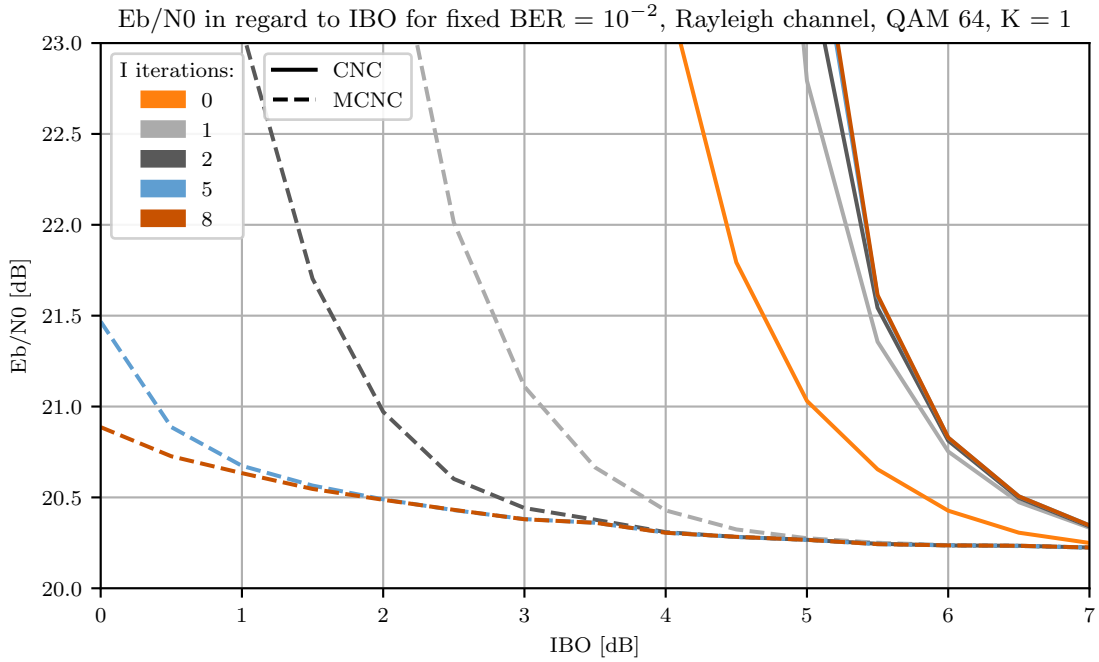

FIGURE 4.15: Eb/N0 in regard to IBO for a fixed BER = 10^{-2}, K = 1 antenna, Rayleigh channel and a selected number of iterations of the CNC and MCNC algorithms.

Chapter 5

Summary

5.1 Conclusions

In this work, the influence of nonlinear distortion on the M-MIMO system has been studied. A mathematical model of the system was presented taking into consideration precoding and front-end nonlinearity. The simulation results provided insight into the radiation patterns of wanted and distortion signal components in the M-MIMO scenario. Moreover, the SDR was analyzed for a LOS, two-path and Rayleigh channels and a selected number of antennas. The analysis allowed to observe that in direct visibility channels the increase in the number of antennas does not improve the SDR and nonlinear distortion is still a major concern as it is beamformed in the same direction as the desired signal. The study of the Multi-user precoding in M-MIMO allowed emphasize that the considered single-user precoding in the presence of nonlinearity is indeed the worst-case scenario.

While it was observed that nonlinear distortion can result in significant M-MIMO performance degradation, a Multi-antenna Clipping Noise Cancellation algorithm was proposed, to combat the problem at the receiver. A starting point for its design was CNC algorithm intended for SISO systems in [11]. While MCNC is complex and computationally demanding a simplified version was proposed a MCNC for flat fading channels. Finally, by the means of extensive simulation, the performance of CNC and MCNC algorithms have been compared and evaluated in regard to a number of parameters. The proposed simplified algorithm proved to perform well for LOS and two-path channels with only slight degradation in regard to MCNC, which may leverage its implementation in the M-MIMO OFDM receivers.

Key findings:

- The problem of nonlinear distortion is still relevant even in multi-antenna scenarios. Especially in direct visibility channels with low scattering the effective beam patterns, i.e., after precoding, of desired and distortion signal components have similar shapes, resulting in an unfavorable signal to distortion ratio.

- The increase in the number of antennas does not improve the SDR for LOS and two-path channels. Only for the ideal Rayleigh channel, the SDR is improved by increasing the number of antennas. This observation highlights the need for distortion removal methods in direct visibility scenarios or when the channel scattering is limited. One of the technologies that can be expected to work with LOS channels and highly nonlinear hardware are millimeter wave (mmW) communications [38].

- Effects of distortion of signal in OFDM system can be mitigated with the use of proper clipping noise recovery algorithms. Proposed in this work Multi-antenna Clipping Noise Cancellation algorithm effectively reduces the nonlinear distortion from the received signal in a M-MIMO system. Later proposed simplification of the MCNC algorithm, requires much less computational resources and performs relatively well with a slight degradation for LOS and two-path channels.
- The performance of the CNC algorithm can be degraded in some cases if the receiver is not aware of the multi-antenna precoding. The proposed MCNC algorithm allows to eliminate this penalty at the expense of increased computational complexity.
- Obtained simulation result allows for comparison of the CNC and Multi-antenna CNC algorithms against a number of parameters Eb/N0, IBO or number of antennas visualizing the gains.

5.2 Future works

Ideas for future development:

- The influence of nonlinearity on the multi-antenna system in terms of signal-to-distortion ratio and effective radiation characteristic could be extended for different types of channels. For example ITU Pedestrian channel model.
- Single user scenario considered in this work is the worst case in terms of SDR. It may be interesting to evaluate the radiation characteristic and the performance of the reception algorithms for the Multi-User MIMO scenarios with a greater number of users.
- The MRT precoding and MCNC algorithm rely on channel state information, however, the perfect channel knowledge is unattainable. A study addressing the impact of CSI accuracy on system performance may provide beneficial insights.
- The proposed MCNC algorithm complexity may be prohibitive in some scenarios. Simplifications regarding the processing steps or accuracy of operations should be considered to leverage the application of the algorithm in mobile devices.

Acronyms

2G	Second generation technology standard for cellular networks
5G	Fifth generation technology standard for broadband cellular networks
6G	Sixth generation technology standard for broadband cellular networks
AI	Artificial Intelligence
BER	Bit Error Rate
BLAST	Bell-Labs Layered Space-Time Architecture
CAF	Clipping and Filtering
CNC	Clipping Noise Cancellation
CORDIC	COordinate Rotation DIgital Computer
CP	Cyclic Prefix
CRAN	Cloud-Based Radio Access Network
CSI	Channel State Information
DAR	Decision Aided Reconstruction
DFT	Discrete Fourier Transform
FD	Frequency Domain
FFT	Fast Fourier Transform
IBO	Input Back-off
IFFT	Inverse Fast Fourier Transform
IoT	Internet of Things
ITU-R	International Telecommunication Union – Radiocommunication Sector
LOS	Line-of-Sight
M-MIMO	Massive MIMO
MCNC	Multi antenna Clipping Noise Cancellation
MIMO	Multiple-input multiple-output
MISO	Multiple-input single-output
ML	Machine Learning
mmW	Millimeter Wave
MRT	Maximum Ratio Transmission
OFDM	Orthogonal Frequency-Division Multiplexing
OSTBC	Linear Space Time-Block Codes
PA	Power Amplifier
PAPR	Peak-to-Average Power Ratio
PSD	Power Spectral Density
QAM	Quadrature Amplitude Modulation
QoS	Quality of Service
RX	Receive/Receiver

SDMA	Space-division multiple access
SDR	Signal-to-Distortion Ratio
SIC	Successive Interference Cancellation
SISO	Single-input Single-output
SM-MIMO	Spatial Modulation MIMO
SNR	Signal-to-Noise Ratio
STTC	Space-Time Trellis Codes
TD	Time Domain
TDD	Time Division Duplex
TX	Transmit/Transmitter
ULA	Uniform Linear Array
ZF	Zero-forcing

Bibliography

[1] Sina Rezaei Aghdam and Thomas Eriksson. On the Performance of Distortion-Aware Linear Receivers in Uplink Massive MIMO Systems. In *2019 16th International Symposium on Wireless Communication Systems (ISWCS)*, pages 208–212, 2019.

[2] Ian F. Akyildiz, Shuai Nie, Shih-Chun Lin, and Manoj Chandrasekaran. 5G roadmap: 10 key enabling technologies. *Computer Networks*, 106:17 – 48, 2016.

[3] A. Al-Hinai and M. Ibnkahla. Neural Network Nonlinear MIMO Channel Identification and Receiver Design. In *2008 IEEE International Conference on Communications*, pages 835–839, 2008.

[4] Cisco and/or its affiliates. Cisco Annual Internet Report (2018–2023). Technical report, Cisco, 2020. Available at `www.cisco.com/c/en/us/solutions/collateral/executive-perspectives/annual-internet-report/white-paper-c11-741490.pdf`.

[5] Lauri Anttila, Alberto Brihuega, and Mikko Valkama. On Antenna Array Out-of-Band Emissions. *IEEE Wireless Communications Letters*, 8(6):1653–1656, 2019.

[6] A. Behravan and T. Eriksson. Papr and other measures for ofdm systems with nonlinearity. In *The 5th International Symposium on Wireless Personal Multimedia Communications*, volume 1, pages 149–153 vol.1, 2002.

[7] Emil Björnson, Jakob Hoydis, Marios Kountouris, and Mérouane Debbah. Massive MIMO Systems With Non-Ideal Hardware: Energy Efficiency, Estimation, and Capacity Limits. *IEEE Transactions on Information Theory*, 60(11):7112–7139, 2014.

[8] Emil Björnson, Jakob Hoydis, and Luca Sanguinetti. Massive MIMO Networks: Spectral, Energy, and Hardware Efficiency. *Foundations and Trends in Signal Processing*, 11(3-4):154–655, 2017.

[9] Richard E. Blahut. *Fast Algorithms for Signal Processing*. Cambridge University Press, 2010.

[10] Vivek Ashok Bohara and See Ho Ting. Theoretical analysis of OFDM signals in nonlinear polynomial models. In *2007 6th International Conference on Information, Communications & Signal Processing*, pages 1–5, 2007.

[11] Hangjun Chen and A.M. Haimovich. Iterative estimation and cancellation of clipping noise for OFDM signals. *IEEE Communications Letters*, 7(7):305–307, 2003.

[12] Maha Cherif and Ridha Bouallegue. The NDIC Algorithm of HPA Nonlinearity on MU-Massive MIMO System Performance. In *2020 International Conference on Software, Telecommunications and Computer Networks (SoftCOM)*, pages 1–4, 2020.

[13] Ericsson. Ericsson Mobility Report. Technical report, Ericsson, 2022. Available at `https://www.ericsson.com/49d3a0/assets/local/reports-papers/mobility-report/documents/2022/ericsson-mobility-report-june-2022.pdf`.

[14] Khaled M. Gharaibeh. *Nonlinear Distortion in Wireless Systems: Modeling and Simulation with MATLAB*. John Wiley & Sons, New York, 2011.

[15] Marco Giordani, Michele Polese, Marco Mezzavilla, Sundeep Rangan, and Michele Zorzi. Toward 6G Networks: Use Cases and Technologies. *IEEE Communications Magazine*, 58(3):55–61, 2020.

[16] Sara Gunnarsson, Jose Flordelis, Liesbet Van der Perre, and Fredrik Tufvesson. Channel hardening in massive mimo-a measurement based analysis. In *2018 IEEE 19th International Workshop on Signal Processing Advances in Wireless Communications (SPAWC)*, pages 1–5, 2018.

[17] Seung Hee Han and Jae Hong Lee. An overview of peak-to-average power ratio reduction techniques for multicarrier transmission. *IEEE Wireless Communications*, 12(2):56–65, 2005.

[18] E. Hossain and M. Hasan. 5G cellular: key enabling technologies and research challenges. *IEEE Instrumentation Measurement Magazine*, 18(3):11–21, 2015.

[19] Dukhyun Kim and G.L. Stuber. Clipping noise mitigation for OFDM by decision-aided reconstruction. *IEEE Communications Letters*, 3(1):4–6, 1999.

[20] Noura Derria Lahbib, Maha Cherif, Moez Hizem, and Ridha Bouallegue. BER Analysis and CS-Based Channel Estimation and HPA Nonlinearities Compensation Technique for Massive MIMO System. *IEEE Access*, 10:27899–27911, 2022.

[21] Erik G. Larsson and Liesbet Van Der Perre. Out-of-Band Radiation From Antenna Arrays Clarified. *IEEE Wireless Communications Letters*, 7(4):610–613, 2018.

[22] Xiaodong Li and L.J. Cimini. Effects of clipping and filtering on the performance of OFDM. *IEEE Communications Letters*, 2(5):131–133, 1998.

[23] Thomas L. Marzetta, Erik G. Larsson, Hong Yang, and Hien Quoc Ngo. *Fundamentals of Massive MIMO*. Cambridge University Press, 2016.

[24] MathWorks. Compute Square Root Using CORDIC, 2022. Available at `https://www.mathworks.com/help/fixedpoint/ug/compute-square-root-using-cordic.html`.

[25] Jan Mietzner, Robert Schober, Lutz Lampe, Wolfgang H. Gerstacker, and Peter A. Hoeher. Multiple-antenna techniques for wireless communications - a comprehensive literature survey. *IEEE Communications Surveys & Tutorials*, 11(2):87–105, 2009.

[26] Christopher Mollen, Erik G. Larsson, Ulf Gustavsson, Thomas Eriksson, and Robert W. Heath. Out-of-Band Radiation from Large Antenna Arrays. *IEEE Communications Magazine*, 56(4):196–203, 2018.

[27] Christopher Mollén, Ulf Gustavsson, Thomas Eriksson, and Erik G. Larsson. Spatial Characteristics of Distortion Radiated From Antenna Arrays With Transceiver Nonlinearities. *IEEE Transactions on Wireless Communications*, 17(10):6663–6679, 2018.

[28] Athanasios Papoulis and S. U. Pillai. *Probability, random variables and stochastic processes*. Tata McGraw-Hill Education, 2002.

[29] K.K. Parhi and T. Nishitami. *Digital Signal Processing for Multimedia Systems*. Signal Processing and Communications. CRC Press, 2018.

[30] J.G. Proakis and D.G. Manolakis. *Digital Signal Processing: Pearson New International Edition*. Pearson Education, 2013.

[31] R. Raich, Hua Qian, and G.T. Zhou. Optimization of SNDR for amplitude-limited nonlinearities. *IEEE Transactions on Communications*, 53(11):1964–1972, 2005.

[32] François Rottenberg, Gilles Callebaut, and Liesbet Van der Perre. Z3RO Precoder Canceling Nonlinear Power Amplifier Distortion in Large Array Systems. In *ICC 2022 - IEEE International Conference on Communications*, pages 432–437, 2022.

[33] H. E. Rowe. Memoryless nonlinearities with Gaussian inputs: Elementary results. *The Bell System Technical Journal*, 61(7):1519–1525, 1982.

[34] Walid Saad, Mehdi Bennis, and Mingzhe Chen. A Vision of 6G Wireless Systems: Applications, Trends, Technologies, and Open Research Problems. *IEEE Network*, 34(3):134–142, 2020.

[35] Da-Shan Shiu and M. Kahn. Layered space-time codes for wireless communications using multiple transmit antennas. In *1999 IEEE International Conference on Communications (Cat. No. 99CH36311)*, volume 1, pages 436–440 vol.1, 1999.

[36] Ying Sun and Hideki Ochiai. Performance Analysis and Comparison of Clipped and Filtered OFDM Systems With Iterative Distortion Recovery Techniques. *IEEE Transactions on Wireless Communications*, 20(11):7389–7403, 2021.

[37] Intenational Telecommunication Union. IMT Vision –Framework and overall objectives of the future development of IMT for 2020 and beyond. Technical report, Intenational Telecommunication Union, 2015. Available at `https://www.itu.int/dms_pubrec/itu-r/rec/m/R-REC-M.2083-0-201509-I!!PDF-E.pdf`.

[38] Xiong Wang, Linghe Kong, Fanxin Kong, Fudong Qiu, Mingyu Xia, Shlomi Arnon, and Guihai Chen. Millimeter wave communication: A comprehensive survey. *IEEE Communications Surveys & Tutorials*, 20(3):1616–1653, 2018.

[39] Shuangqing Wei, Dennis L. Goeckel, and Patrick A. Kelly. Convergence of the Complex Envelope of Bandlimited OFDM Signals. *IEEE Transactions on Information Theory*, 56(10):4893–4904, 2010.

[40] Hyunseuk Yoo, Frédéric Guilloud, and Ramesh Pyndiah. Probability distribution analysis of M-QAM-modulated OFDM symbol and reconstruction of distorted data. *EURASIP Journal on Advances in Signal Processing*, 2011(135), 2011.

[41] Zhengquan Zhang, Yue Xiao, Zheng Ma, Ming Xiao, Zhiguo Ding, Xianfu Lei, George K. Karagiannidis, and Pingzhi Fan. 6G Wireless Networks: Vision, Requirements, Architecture, and Key Technologies. *IEEE Vehicular Technology Magazine*, 14(3):28–41, 2019.

Poznan University of Technology
Faculty of Computing and Telecommunications
Institute of Radiocommunications

Typeset using LaTeX.